Particle Accelerators, 1972, Vol. 3, pp. 129–161

ESTIMATION OF RADIATION PROBLEMS AROUND HIGH ENERGY ACCELERATORS USING CALCULATIONS OF THE HADRONIC CASCADE IN MATTER

J. RANFT

Sektion Physik, Karl-Marx-Universität, Leipzig, DDR

Monte Carlo calculations of the hadronic extranuclear cascade are described. These calculations are applied to a variety of radiation problems around high energy accelerators, for instance: estimation of shielding requirements, induced radioactivity, direct radiation doses and radiation heating. Good agreement, usually better than within a factor two, is found with experimental data at present accelerators.

1. INTRODUCTION

The investigation of hadronic and electromagnetic cascades is of considerable interest for all aspects of radiation physics around high energy proton accelerators. The primary proton interactions induce the development of hadronic and electromagnetic cascades which transport and deposit the energy of the interacting particles in matter. The experimental investigation of hadronic cascades has been performed during the past few years with incident protons of momenta up to 24 GeV/c mainly for concrete, earth and steel, as shielding materials.[1–7]

These experiments were recently reviewed and evaluated by Patterson and Thomas.[8] The most important radiation problems around present and future high energy proton accelerators are described in Ref. 9.

Theoretical cascade calculations can be divided into two groups:

To the first group belong essentially one dimensional analytical cascade calculations[10–28] which cannot always be directly compared with experimental data; the second group consists of Monte Carlo calculations of the three-dimensional development of the cascade.[29–60]

The results of the two approaches are in mutual agreement and in addition they are consistent with the experimental results obtained at present accelerators.

The development of the cascades especially in the GeV energy region is not yet completely understood. The main features of the cascade, which are relevant for assessing the radiation problems, are however sufficiently well known. The transport and spatial distribution of the cascade in shielding materials and in the material of accelerator components are determined from the cascade of hadronic particles with energies above one hundred MeV. The dominant mechanism of energy deposition at several hundred GeV is, however, the electromagnetic cascade induced by the decay of π^0-mesons into gammas. The radiation transport in transverse direction with respect to the primary beam is determined by the hadronic cascade. In the forward direction, however, the shielding requirements are determined by penetrating muons from the decay of charged π and K mesons.

The essential physical assumptions which enter into the cascade calculations at GeV energies are:

(i) The absorption cross sections of hadrons on nuclei which are assumed to remain constant above 20 GeV. This assumption is in agreement with most of the current theoretical models and with cosmic ray experiments.

(ii) The momentum spectra of hadronic secondaries created in hadron nucleus collisions are described in calculations usually by empirical or semiempirical extrapolation formulae. These are then fitted to experimental data at present accelerator energies.

These and other relevant physical input data are described in detail in Sec. 2.

Cascade calculations are preferably performed in simple geometrical situations with some kind of symmetry. Most situations around high energy accelerators, where high energy protons interact with machine components, are rather complicated. Under such conditions the calculation can be simplified by using a two step procedure. First we study the interaction of primary protons in ejection septa, targets, or beam scrapers (the most important sources of beam loss inside an accelerator or beam line). From these losses we calculate a linear particle loss distribution in the accelerator or beam line.

This distribution of protons lost along the vacuum tube serves in a second stage of the calculation as the starting point for the Monte Carlo calculation of the hadronic cascade in magnets and shielding walls around the beam with simplified assumptions concerning the geometrical layout. The calculation of the loss distribution is described in Sec. 3.2. Some of the most useful results of cascade calculations relevant to radiation problems are the following:

(i) The flux density of particles is used to determine the necessary shielding dimensions.

(ii) The density of hadronic interactions (hadronic cascade star density) is closely related to the induced radioactivity.

(iii) The energy deposition density in the material is equivalent to the direct radiation dose or the heat deposited in the material.

In Sec. 3.3 we describe the Monte Carlo calculation[29–45] of the hadronic cascade. Results of these calculations are discussed in Sec. 4. Analytical cascade calculations are briefly reviewed in Sec. 5.

2. PHYSICAL DATA DESCRIBING THE INTERACTION OF PARTICLES WITH MATTER

2.1. *Absorption Cross Sections*

Absorption cross sections of protons, neutrons and pions on nuclei for energies between tens of MeV and hundreds of GeV are needed for the calculations. The dependence of the cross sections on the target nucleus can usually be represented in the form $\sigma_{\text{abs}} = \sigma_0 A^B$, where A is the atomic weight of the nucleus. Using data from Ref. 73 at $p_0 \approx 20$ GeV/c one finds

$$\sigma_{\text{abs}}(A) = 50.4 A^{0.67} \text{ mb}. \tag{2.1}$$

It should, however, be noted that the absorption cross section on hydrogen $\sigma_{\text{abs}}(A = 1) = 31.5$ mb is smaller than would follow from (2.1).

In the resonance region below a few GeV the cross sections are energy dependent. Above this region up to the highest now accessible accelerator energies[61,62] the cross sections remain nearly constant. Most cosmic ray experiments report energy independent cross sections up to the highest energies, but there was recently also a report on proton cross sections rising with energy.[63,64] Proton and pion absorption cross sections on different nuclei between 50 MeV and 30 GeV were reviewed by Barashenkov *et al.*[65,66] and by the HERA group.[67–72] Recent experimental results are reported in Ref. 73 for protons, in Refs. 74 and 75 for neutrons, and in Ref. 61 for pions. Neutron and pion cross sections are smaller than proton cross sections,[34] and at energies above a few GeV, one might use

$$\begin{aligned} \sigma_{nN} &= \sigma_{pN}/1.07 \\ \sigma_{\pi N} &\quad \sigma_{pN}/1.20. \end{aligned} \tag{2.2}$$

For target materials, where no measurements are available, we use the interpolation

$$\begin{aligned} \sigma(A) &= \sigma_1 \left(\frac{A}{A_1}\right)^B \\ B &= \log\left(\frac{\sigma_2}{\sigma_1}\right) \Big/ \log\left(\frac{A_2}{A_1}\right), \end{aligned} \tag{2.3}$$

where σ_1 and σ_2 are the known cross sections for nuclei with atomic weights A_1 and A_2 respectively. The cross sections above 10 GeV as given in Refs. 65 and 66, which are used in the calculation, are smaller than those reported in Ref. 73. Using the lower values in the cascade calculation is advisable for a conservative estimate of the shielding requirements.

The absorption length used in the calculations is defined by

$$\lambda_{\text{abs}}(A) = \frac{A}{\sigma_{\text{abs}} \cdot N} \text{ (g/cm}^2\text{)}, \tag{2.4}$$

where $N = 6.022 \cdot 10^{23}$ is the Avogadro number.

2.2. *Elastic Scattering*

The total elastic cross sections measured by Bellettini *et al.*[73] can be represented empirically by[76]

$$\sigma_{\text{tot.el}}(A) = 6.38 A^{1.04} \text{ mb} \tag{2.5}$$

and we use an elastic scattering length

$$\lambda_{\text{el}}(A) = \frac{A}{\sigma_{\text{tot.el}}(A) \cdot N} \text{ (g/cm}^2\text{)}. \tag{2.6}$$

The total elastic cross sections increase faster with A than the absorption cross sections. For proton–proton collisions we have a ratio:

$$\sigma_{\mathrm{abs}}(pp):\sigma_{\mathrm{tot.el}}(pp)=3:1, \tag{2.7}$$

but for Pb the ratio is nearly 1:1 with $\sigma_{\mathrm{abs}}(\mathrm{Pb}) = 1750$ mb, and $\sigma_{\mathrm{tot.el}}(\mathrm{Pb}) = 1540$ mb. This behaviour can also be seen from (2.1) and (2.5) which give

$$\sigma_{\mathrm{tot.el}}(A)/\sigma_{\mathrm{abs}}(A) \approx A^{0.37}.$$

The total elastic cross sections are assumed to be independent of the primary proton momentum.

The differential elastic cross sections can be represented as sums of Gaussians, which are rather convenient for the random selection of scattering angles in Monte Carlo calculations.[76] The data of Ref. 73 are well represented for $A < 62$ by

$$\frac{\mathrm{d}\sigma_{\mathrm{el}}}{\mathrm{d}\Omega} \approx A^{1.63}\exp(14.5\cdot A^{0.66}t) + 1.4A^{0.33}\exp(10t) \tag{2.8}$$

where the momentum transfer t (measured in units of $(\mathrm{GeV/c})^2$) is defined as $t = -2p^2(1-\cos\theta)$, p and θ are momentum and angle of the scattered particle; t can be approximated by $t \approx -p^2\theta^2$ since the angles θ are rather small. Above $A = 62$ the structure of the cross section is more complicated. We use instead a simple form similar to (2.8) without secondary diffraction maxima:

$$\frac{\mathrm{d}\sigma_{\mathrm{el}}}{\mathrm{d}\Omega} \approx A^{1.33}\exp(60\cdot A^{0.33}t) + 0.4A^{0.40}\exp(10t). \tag{2.9}$$

The absolute normalization of the differential cross sections (2.8) and (2.9) is not important for the selection of random scattering angles. The cross sections might however be normalized using (2.5) if required.

2.3. *Multiple Particle Production*

There has been much interest in particle production in hadron–hadron collisions during the past few years. Experimental measurements mainly for pp collisions were reported from all the larger accelerators. Theoretical efforts were concentrated on the development of models for multi-particle production and on the asymptotic behaviour of the production cross sections. Presently the thermodynamic model[77–79] describes for p–p collisions practically all the data available at accelerator energies and predicts the particle production at higher energies. Data on pion and proton production are explained equally well by the multi-Regge-model.[80,81]

The scaling conjecture of Feynman[82,83] and the hypothesis of limiting fragmentation[84] predict the asymptotic behaviour. The discovery of Mueller[85] that inclusive cross sections are related to discontinuities of elastic multiparticle scattering amplitudes was the starting point for the application of Regge phenomenology[86] and dual models[87,88] to inclusive multiparticle production. Most of these theoretical approaches were recently reviewed in Ref. 89. The most important gap in the knowledge, experimental as well as theoretical, concerns the production of all kinds of secondary particles in collisions other than p–p or p–nucleus, especially in π–N collisions, where not much data are presently available. Furthermore a quantitative understanding of the production of secondaries in hadron-nucleus-collisions is needed.

For the Monte Carlo calculations which are of interest to us, we need simple formulae (which permit the fast selection of random secondary particle momenta and angles) describing the momentum spectra of secondary protons, neutrons and pions in collisions of protons, pions and neutrons with nuclei. Empirical formulae, which represent known accelerator data reasonably well and which behave at higher energies qualitatively as demonstrated by the theoretical models, are most useful for this task. The first empirical formula for pion production was proposed by Cocconi, Koester and Perkins.[90,91] Other formulas were proposed later for pion and proton production and fitted to experimental data.[92–94] Most of the empirical formulae are described in Ref. 95. The Trilling and modified Trilling formulae for pion and proton production which were fitted to data in p–nucleus collisions[96] and were used most often in past cascade calculations. These formulae are described in the following.

Measured data are usually given as

$$\frac{\mathrm{d}^2\sigma}{\mathrm{d}p\,\mathrm{d}\Omega}\left[\frac{\mathrm{mb}}{\mathrm{GeV/c,\ sr}}\right] \tag{2.10}$$

but we need the spectra in the form

$$\frac{d^2N}{dp\,d\Omega}\left[\frac{\text{number of particles}}{\text{GeV/c, sr, interacting proton}}\right] = \frac{d^2\sigma}{dp\,d\Omega}\cdot\frac{1}{\sigma_{abs}}. \tag{2.11}$$

For σ_{abs} we use the data of Ref. 73

$$\begin{aligned}\sigma_{abs}(\mathrm{H}) &= 31.5 \text{ mb}\\ \sigma_{abs}(\mathrm{Be}) &= 227 \text{ mb}\\ \sigma_{abs}(\mathrm{Al}) &= 472 \text{ mb}\\ \sigma_{abs}(\mathrm{Cu}) &= 850 \text{ mb}\\ \sigma_{abs}(\mathrm{Pb}) &= 1750 \text{ mb}.\end{aligned}$$

For the production of nucleons in nucleon–nucleus-collisions we use the improved Trilling formula:

$$\begin{aligned}\frac{d^2N}{dp\,d\Omega} = &\left[\frac{A_1}{p_0}\left(1+\frac{A_4}{(1+p)}+\frac{1.5A_4}{(1+p^2)}\right)\right.\\ &+\frac{A_2\,p}{p_0^{\,2}}\left|1+\left(1+\left(\frac{p_0}{m_p}\right)^2\right)^{1/2}\right.\\ &\left.-\frac{p_0}{p}\left(1+\left(\frac{p}{m_p}\right)^2\right)^{1/2}\right|\Bigg]\\ &\cdot p^2\left[1+\left(1+\left(\frac{p_0}{m_p}\right)^2\right)^{1/2}\right.\\ &\left.-\frac{p_0\,p}{m_p^{\,2}(1+(p/m_p)^2)^{1/2}}\right]\\ &\cdot\exp(-A_3\,p^2\theta^2)\end{aligned} \tag{2.12}$$

where p_0 is the primary proton momentum and p and θ are momentum and angle of the secondary particles.

The parameters A_1 to A_4, as taken from Ref. 95 or 39 are given in Table 2.I. The parameters for other target materials are determined by interpolation. For pion production the Trilling formula is used

$$\begin{aligned}\frac{d^2N}{dp\,d\Omega} = &A_1\,p^2\exp(-A_2\,pp_0^{-1/2}-A_3\,pp_0^{1/2}\,\theta^2)\\ &+A_4\frac{p^2}{p_0}\exp\left(-A_5\left(\frac{p}{p_0}\right)^2-A_6\,p\theta\right).\end{aligned} \tag{2.13}$$

The available data at 19.2 GeV/c[96] are not sufficient to determine all six parameters uniquely. Therefore the parameters A_2 and A_3 were kept the same for all target materials as determined from the data in *p-p* collisions. The data[96] are mainly for large secondary momenta p where the second term of the Trilling formula dominates. Due to this reason we cannot expect the formula to represent the pion production very well at small secondary momenta. Parameters A_1 to A_6[39] are given in Table 2.II. The π^0 spectrum is expected to be somewhere between the π^+ and π^- spectra.

TABLE 2.I
Parameters of the improved Trilling formula for *p*-production obtained by a fit to data at 19.2 GeV/c (Ref. 30)

Target	A_1	A_2	A_3	A_4
H	0.885	0.101	4.256	0
Be	0.756	−0.192	4.058	0.2
Al	0.856	−0.555	3.902	0.5
Cu	0.855	−0.712	3.759	1.0
Pb	0.744	−0.730	3.580	2.0

TABLE 2.II
Parameters of the Trilling formula for $\pi^\pm$ production in *p*–nucleus collisions, obtained by a fit to data at 19.2 GeV/c (Ref. 30)

Target	Particle	A_1	A_2	A_3	A_4	A_5	A_6
H_2	π^+	3.39	4.15	4.56	7.14	9.6	4.82
	π^-	3.39	4.15	4.56	1.85	9.6	4.82
Be	π^+	3.52	4.15	4.56	3.49	9.9	4.04
	π^-	3.52	4.15	4.56	1.01	9.9	4.04
Al	π^+	3.88	4.15	4.56	3.04	10.0	3.91
	π^-	3.88	4.15	4.56	0.82	10.0	3.91
Cu	π^+	4.13	4.15	4.56	2.47	9.7	4.01
	π^-	4.13	4.15	4.56	0.67	9.7	4.01
Pb	π^+	3.43	4.15	4.56	1.88	9.9	3.85
	π^-	3.43	4.15	4.56	0.56	9.9	3.85

At large angles or transverse momenta the proton and pion production according to these formulae drops much faster with increasing angle than the spectra according to the thermodynamic model. If the production at large angles is of interest, it is therefore advisable to use the thermodynamic model spectra. The spectra according to the thermodynamic model agree well with data up to nearly $\theta = 90°$. They describe, however, only the particle production in *p–p* collisions, not in *p*–nucleus collisions. Particle spectra in hadron nucleus collisions are the ones needed for cascade calculations.

Experimental data, however, are available only for rather large secondary momenta ($p > 0.25\, p_0$) and from small angles ($\theta < 20°$).

The secondary particle spectra at small momenta p and large angles θ differ strongly from those in p–p collisions because of the intranuclear cascade and nuclear evaporation. Caution is required because of this lack of experimental as well as theoretical information for the large angle, small secondary momentum spectra. If the cascade develops in a sufficiently large mass, it is believed that the effect of the cascade dominates finally. If no cascade development takes place the actual particle fluxes might differ at large angles by large factors from the predictions of the empirical Trilling formulae.

For future cascade calculations it is more advantageous to describe particle production by empirical formulae with Feynman scaling behaviour. We use formulae similar to the ones described by Bali *et al.*[83] and Bøggild, Hansen and Suk.[97] These formulae are defined in the p–p c.m.s. frame using the longitudinal momentum $p_{\parallel}{}^*$ and the transverse momentum $p_\perp$ (both in GeV/c), the total c.m.s. energy (of p–p) being E_{CM} (in GeV).

Pion production is described by

$$\frac{d^2N^*}{\mathrm{d}p_{\parallel}{}^*\,\mathrm{d}p_\perp} = \frac{U\exp[-(A/E_{\mathrm{CM}}^2)p_{\parallel}^{*2}]\cdot p_\perp[\exp(-Bp_\perp{}^2)+C\exp(-Dp_\perp)}{(p_{\parallel}^{*2}+p_\perp{}^2+m_\pi{}^2)^{1/2}} \left[\frac{\text{number of particles}}{(\mathrm{GeV/c})^2,\ \text{interacting proton}}\right]. \tag{2.14}$$

The parameters U, A, B, C and D were fitted to experimental data and are given in Table 2.III where m_π is the mass of the pion (in GeV/c^2).

Secondary nucleon production is described by

$$\frac{d^2N^*}{\mathrm{d}p_{\parallel}{}^*\,\mathrm{d}p_\perp} = \frac{Q}{E_{\mathrm{CM}}}\left[1+\frac{V}{E_{\mathrm{CM}}}p_{\parallel}{}^*+\frac{W}{E_{\mathrm{CM}}^2}p_{\parallel}^{*2}\right]\cdot p_\perp[\exp(-Bp_\perp{}^2)+C\exp(-Dp_\perp)] \left[\frac{\text{number of particles}}{(\mathrm{GeV/c})^2,\ \text{interacting proton}}\right]. \tag{2.15}$$

TABLE 2.III
Parameters of the formula (2.14)

Particle	Target material	U	A	B	C	D
π^+	H_2	4.94	33.83	6.11	0.69	4.12
π^+	Be	1.81	33.39	3.01	5.12	7.34
π^+	Al	1.54	35.54	3.70	3.03	4.94
π^+	Cu	2.36	37.21	5.83	0.76	3.22
π^+	Pb	1.79	38.60	6.04	0.96	3.23
π^-	H_2	2.81	44.08	5.17	0.81	4.34
π^-	Be	1.52	42.74	5.33	0.82	3.53
π^-	Al	1.54	44.62	5.67	0.83	3.17
π^-	Cu	1.60	46.52	6.47	0.93	3.05
π^-	Pb	1.55	47.16	6.02	0.50	2.66

The fitted values of the parameters Q, V, W, B, C and D are given in Table 2.IV for different target materials. Parameters for other materials can be determined by interpolation.

The random selection of $p_{\parallel}{}^*$ and $p_\perp$ in the c.m.s. using the formulae (2.14) or (2.15) can be done efficiently. The laboratory frame momenta and angles are determined by a Lorentz transformation. It is necessary to add to (2.14) and (2.15) contributions describing the effects of the intranuclear

TABLE 2.IV
Parameters of formula (2.15) describing proton production

Target material	Q	V	W	B	C	D
H_2	8.71	0.86	−3.37	3.78	0.47	3.60
Be	2.65	1.03	−3.85	5.63	3.49	2.89
Al	2.76	−2.99	4.90	3.91	5.82	2.99
Cu	8.87	−1.78	0.30	5.38	0.38	1.41
Pb	3.10	1.01	−8.66	4.65	1.79	2.47

cascade and nuclear evaporation at small laboratory momenta of the secondaries. The formulae (2.14) and (2.15) will be described in more detail in Ref. 98.

2.4. *Multiple Coulomb Scattering and Ionization Energy Losses*

The Rossi formula is sufficient for the Monte Carlo calculations envisaged. A Gaussian angular distribution of the scattering angles is assumed with r.m.s. projected angles given by

$$\langle\theta^2\rangle^{1/2} = \frac{15\,[\mathrm{MeV}]}{p\beta c\,[\mathrm{MeV}]}\left(\frac{l}{l_{\mathrm{rad}}}\right)^{1/2}(1-\varepsilon)\,[\mathrm{rad}] \quad (2.16)$$

where l_{rad} is the radiation length of the material considered. ε is a correction factor approximated by

$$\varepsilon = 0.14 - 0.06\ln(l_{\mathrm{rad}}). \quad (2.17)$$

Ionization energy losses are described in detail in Refs. 99, 100.

The stopping power is calculated using the following formula

$$-\frac{\mathrm{d}E}{\mathrm{d}x} = z^2\frac{Z}{A}K(\beta)\left[\rho(\beta) - \ln(I) - \frac{C}{Z} - \frac{\delta}{2}\right]\cdot\left[\frac{\mathrm{MeV}}{\mathrm{g/cm^2}}\right] \quad (2.18)$$

where z is the charge of the incident particle. Z and A are the atomic number and weight of the target material. β is the relativistic velocity $\beta = p/(p^2+m^2)^{1/2}$. The functions $K(\beta)$ and $\rho(\beta)$ are

$$K(\beta) = \frac{0.307}{\beta^2}$$

$$\rho(\beta) = \ln[1.022\cdot 10^6\beta^2/(1-\beta^2)] - \beta^2. \quad (2.19)$$

I is the mean atomic excitation energy of the material measured in eV which is approximately given by[100]

$$I = Z\cdot(12+7/Z)\ \mathrm{eV} \quad \text{for} \quad I < 163\ \mathrm{eV}$$

$$I = Z\cdot(9.76+58.5Z^{-1.19})\ \mathrm{eV} \quad \text{for} \quad I > 163\ \mathrm{eV}. \quad (2.20)$$

The term C/Z is the tight binding or inner shell correction. For

$$\mu = \beta\gamma = \frac{\beta}{\sqrt{1-\beta^2}} \geqq 0.13$$

we have approximately[100]

$$\begin{aligned} C(I,\mu) = {} & (0.422377\mu^2 + 0.0304043\mu^{-4} \\ & -0.00038106\mu^{-6})\times 10^{-6}\,I^2 \\ & +(3.85019\mu^{-2} - 0.1667989\mu^{-4} \\ & +0.00157955\mu^{-6})\times 10^{-9}\,I^3 \end{aligned}$$

δ is the density effect correction, which has to be used for materials in liquid and solid form. Sternheimer[141,142] gives:

$$\begin{aligned} &\delta = 0 && \text{for} \quad x < x_0 \\ &\delta = 4.606 + C_1 + a(x_1 - x)^m && \text{for} \quad x_0 \leqq x \leqq x_1 \\ &\delta = 4.606x + C_1 && \text{for} \quad x > x_1 \\ &x = 0.5\log_{10}[\beta^2/(1-\beta^2)] \end{aligned}$$

where the parameters a, m, C_1 and x_1 are material dependent. The density effect corrections are very important at high energy, where they reduce the stopping power.

2.5. *Electromagnetic Cascades*

Electromagnetic cascades are produced in matter by high-energy electrons and photons. They are a very efficient mechanism for energy deposition in matter, and in this respect also of importance for the hadronic cascade. Experiments on electromagnetic cascades have been done extensively. The results of careful calculations, either analytical or with the Monte Carlo method agree generally within 10 per cent with experimental results. A literature survey may be found in Refs. 101–103.

3. MONTE CARLO CALCULATIONS

3.1. *Different Monte Carlo Cascade Calculations*

Details on Monte Carlo cascade calculations are given in Table 3.I. We treat in the following mainly the principles and results of the programmes 1 to 6 of Table 3.I.† The method of calculation differs in the programmes TRANSK and FLUTRA; other programmes differ only in respect to the geometrical situation. These methods are described in Sec. 3.3.

† All these programmes are written in FORTRAN-IV, programmes 1 to 5 for the CDC-6600-6500, programmes 1, 2 and 6 for the IBM-system 360. They use between 40 and 60 K words of memory. The 1967 version of TRANSK, described in Ref. 37 is available from the CERN Programme library. Programmes 1 to 5 are also available from Dr. J. Routti, CERN Lab. II. Programmes 1, 2 and 6 (IBM 360 versions) are in use at NAL (Radiation physics group, Dr. M. Awschalom).

TABLE 3.I
Monte Carlo calculations of the nucleon meson cascade

No.	Programme	Remarks	References
1	TRANSK	Backstop geometry $50 \text{ MeV} \leqq E \leqq 1000 \text{ GeV}$ particle splitting technique, star densities, energy deposition, muon flux density, angular and momentum distributions, induced activity.	31, 32, 33, 34, 35, 37, 39
2	FLUTRA -FLUKA†	Backstop geometry $50 \text{ MeV} \leqq E \leqq 1000 \text{ GeV}$, more reliable than TRANSK, no particle splitting, star densities, energy deposition, induced activity, performance of ionization, calorimeters—TANC–SANC detectors.	40, 42, 44, 143
3	MAGTRA -MACKA†	Target in front of a synchrotron magnet approximated by a hollow cylinder, otherwise like FLUTRA.	38, 41, 42, 45, 144
4	TASTAK	Target in front of bending magnet (with magnetic field), otherwise like FLUTRA.	42, 45
5	KASTRA	Beam tube, synchrotron magnets (hollow cylinders) and cylindrical shielding wall, otherwise like TRANSK.	36
6	FLUTRA -(HITORM)	Arbitrary geometry specified by routine HITORM, otherwise like FLUTRA.	59
7	NTC	$E < 400$ MeV, absorbed dose, arbitrary geometry.	51, 52, 113
8	NMTC	$E < 3$ GeV, arbitrary geometry absorbed dose, induced activity.	53, 48, 47, 54, 58, 116–20, 138, 139
9	HETC	$E < 1000$ GeV, induced activity, star densities.	114, 115
10	Akimov *et al.*	Ionization calorimeter, design.	50
11	Göllnitz *et al.*	Neutron scattering, chamber design.	49
12	Jones	10–1000 GeV, ionization spectrometer performance.	56, 57
13	Barashenkov *et al.*	50 MeV–100 GeV beam stop geometry, flux density, induced activity.	60

† FLUKA and MACKA use the formulae (2.14) and (2.15) for secondary particle production and are otherwise identical to FLUTRA and MAGTRA.

The cascade calculation in the programmes MAGTRA, TASTAK and KASTRA starts from a linear line source of interacting protons. This line source is calculated by Monte Carlo calculations which are discussed in Sec. 3.2.

There are other Monte Carlo programmes which are not described in detail here. The code NTC calculates the transport of protons and neutrons of energies less than 400 MeV. This code relies on the intranuclear-cascade code of Bertini[121] for particle production in nucleon–nucleus collisions. Recently NTC has been extended to NMTC (Nucleon–Meson Transport Code) which is applicable up to 3 GeV. The results of high energy nucleus–meson cascade calculations carried out with NMTC have been compared with a variety of experimental data and good agreement has been obtained.[138,139] This code was also applied to calculate the production of residual radioactive nuclei by high energy particles and the induced photon dose rates for a variety of situations which are of importance around high energy accelerators. Figure 1 gives such results and compares them with the results obtained by MAGTRA.

Other Monte Carlo calculations[49,50,56,57] of the nucleon–meson cascade at high energies up to the cosmic ray energy region have been performed to estimate the efficiency of ionization calorimeters.[122] These devices are similar to the TANC and SANC detectors which will be described in Sec. 4.4.1.

3.2. *Beam Losses in Accelerators and Beam Lines, the Calculation of an Effective Line Source*

All radiation problems in the main ring of a proton synchrotron originate from wanted and unwanted interactions of protons with machine components. Here we study these interactions. Furthermore the resulting beam loss distributions are studied. In particular the interaction of primary protons in ejection septa, targets, and beam scrapers is considered (the most important sources of beam losses). Using the results obtained, the loss distributions in the ring downstream of these elements are calculated.

The distribution of protons lost along the vacuum tube of the accelerator serves at a later stage as the starting point for a Monte Carlo calculation of the hadronic cascade—with simplified assumptions concerning the geometrical layout—which is used

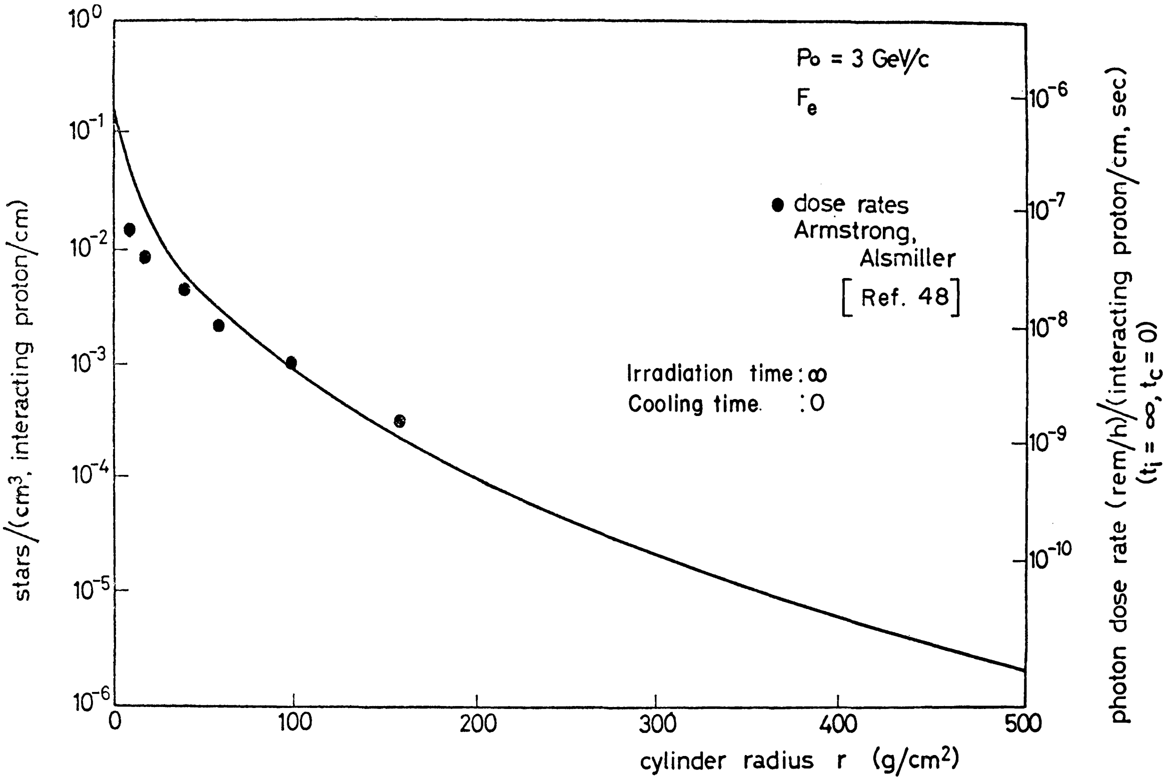

FIG. 1. The radial dependence of the hadronic cascade star densities calculated for 3 GeV/c protons interacting uniformly along the centre of an infinite Fe cylinder.

to estimate the resulting damage and activation of machine components (see Sec. 3.3).

3.2.1. *Scattering of Protons in Septa of Ejection Systems.* We consider different kinds of septa and systems of septa: Magnetic septa with a magnetic field B_0 decreasing linearly to zero over the septum thickness, electrostatic septa with an electric field E_0, and wire septa, consisting of a parallel array of single wires arranged perpendicular to the direction of the proton beam.

The septa are described by material parameters, Z, A, and the density ρ [g/cm³], and by the geometrical parameters, thickness D [cm], length L [cm], and angle θ [rad] relative to the direction of the closed orbit.

The proton beam is described by the proton density along the outgoing separatrices in radial phase space and the angular divergence of the protons.

In a Monte Carlo calculation we consider the scattering of the protons in the septa only in radial phase space. Protons at the upstream end of the first septum are selected randomly. The paths of these protons are followed considering electric and magnetic fields outside the septa. If the protons enter the septa we take elastic and multiple coulomb scattering as well as ionization loss and deflection by magnetic fields into account. Inelastic collisions of the protons with nuclei lead to a continuous decrease of the weight W attributed to each proton.

$$W = W_0 \cdot \exp\left(-\frac{l}{\lambda_{\text{abs}}}\right)$$

where l is the path length inside the septum. The calculation for each proton stops at the downstream end plane of the last septum considered. We represent the results of the calculations by the following quantities.

F_h — the fraction of the proton beam hitting the septum;

F_{ai}	the fractions of protons being absorbed in each septum of the system;
$F_{sc} = F_{out} + F_r$	the fraction of protons scattered out of the septum into the ejection channel F_{out} and back into the main ring F_r;
$\dfrac{d^2N}{dr\,dr'}$	the density distribution of the scattered protons in radial phase space;
$\dfrac{dN}{dr'}$	the angular distribution of the scattered protons;
$\dfrac{dN}{dp}$	the momentum distribution of the scattered protons.

All distributions are normalized to 1 proton entering the ejection channel or hitting the septum.

Results of calculations are reported in Refs. 76, 104, 105; we give here only some results for the CERN-PS septum lens 63, for an electrostatic foil septum at 300 GeV, and for a wire septum as proposed by Maschke[106] at 250 GeV. Tables 3.II to 3.IV give the fractions F_i calculated and Figs. 2 and 3 give the distributions dN/dr' and dN/dp for the electrostatic foil septum at 300 GeV. The results are given as function of the relative orientations of septum and proton beam $\Delta\theta = \theta_{sept} - \theta_{beam}$.

The fraction F_{sc} of protons scattered out of the very thin septa considered can be quite a high fraction of the protons hitting the septa. F_{sc} increases as the septa become thinner and decreases with increasing proton momentum. Two contributions are visible in the distribution dN/dr', the narrow peak comes from multiple Coulomb scattering and the long tail results from elastic scattering. The magnetic and electrostatic fields are the reason for the asymmetries between F_r and F_{out} for $\Delta\theta = 0$ and between the results for positive and negative $\Delta\theta$.

The large fraction of protons scattered out of the septa explains the halo of the ejected proton beam and also the fact that the beam losses are not localized at the septum. The absolute magnitudes of the fractions F_h, F_a, etc. given in the tables might have no real significance, since they change with the density distribution of the protons across the septum. The distributions used in the calculation are rather optimistic.

TABLE 3.II

Results for the CPS septum lens 63. The phase space density of the proton beam along the outgoing separatrix is taken from Ref. 104. The parameters of the septum are: $D = 0.03$ cm, $L = 103$ cm, $B = 0.4$ kG, $B' = -0.64$ kG/cm, the septum material is Cu

$\Delta\theta$ (mrad)	-0.5	-0.25	0	0.25	0.5
F_h(%)	4.67	3.39	1.90	2.18	3.17
F_a(%)	2.40	1.67	1.12	1.21	1.67
F_r(%)	1.23	1.04	0.40	0.51	0.69
F_{out}(%)	0.78	0.56	0.36	0.45	0.79
F_{sc}(%)	2.24	1.71	0.77	0.96	1.49

TABLE 3.III

Results for an electrostatic septum for the 300 GeV accelerator. The septum consists of two parts with a relative orientation $\Delta\theta = 0.02$ mrad, and the following dimensions: $D_1 = D_2 = 0.005$ cm, $L_1 = 120$ cm, $L_2 = 300$ cm, $E_1 = E_2 = 53$ kV. The material is Cu. The beam jump over the septum is 2 cm. The proton density decreases over these 2 cm linearly to two thirds of the value at the septum. The divergence spread of the beam is $\Delta r' = \pm 0.02$ mrad

$\Delta\theta$ (mrad)	-0.04	-0.02	0	0.02	0.04
F_h(%)	0.93	0.52	0.36	0.44	0.77
F_{a1}(%)	0.37	0.29	0.24	0.25	0.33
F_{a2}(%)	0.19	0.05	0.005	0.04	0.16
$F_{a\,tot}$(%)	0.56	0.33	0.25	0.29	0.48
F_r(%)	0.28	0.14	0.06	0.045	0.07
F_{out}(%)	0.07	0.05	0.04	0.10	0.21
F_{sc}(%)	0.36	0.19	0.10	0.14	0.28

TABLE 3.IV

Results of the Monte Carlo calculation of proton scattering in a wire system. The proton momentum is $p_0 = 250$ GeV/c. The parameters of the wire system are: material: W, diameter of wires $d = 0.003$ cm, distance of wires $= 0.1$ cm (1000 wires per metre), length in beam direction $L = 300$ cm. We assume a uniform proton density on the outgoing separatrix, the jump of the protons is 1 cm. The assumed divergence spread is $\Delta\theta = \pm 0.01$ mrad. Z_W is the average length of material (W) traversed by the scattered protons

Misalignment $\Delta\theta$ (mrad)	F_a (%)	Z_W (cm W)	Z_W (No. of wires)	F_r (%)	F_{out} (%)
0	0.085	1.04	350	0.30	0.30
0.04	0.25	0.95	320	0.31	1.5
0.08	0.35	0.85	280	0.35	3.0
-0.08	0.45	0.90	290	3.5	0.3

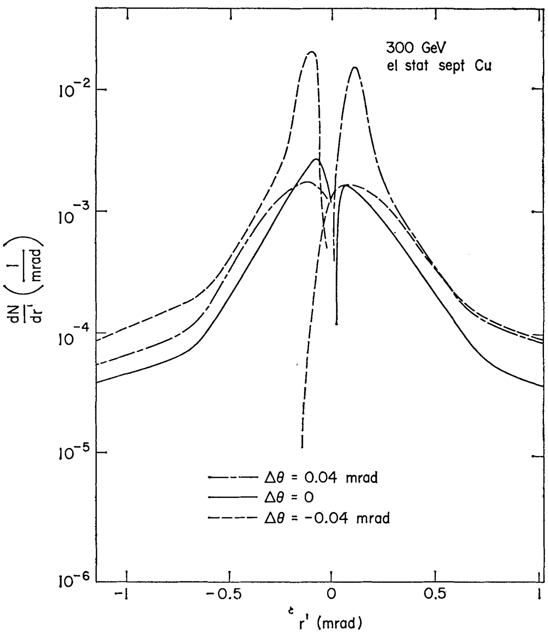

FIG. 2. Angular distribution dN/dr' of protons scattered out of an electrostatic foil septum of the 300-GeV accelerator for different septum misalignments $\Delta\theta$.

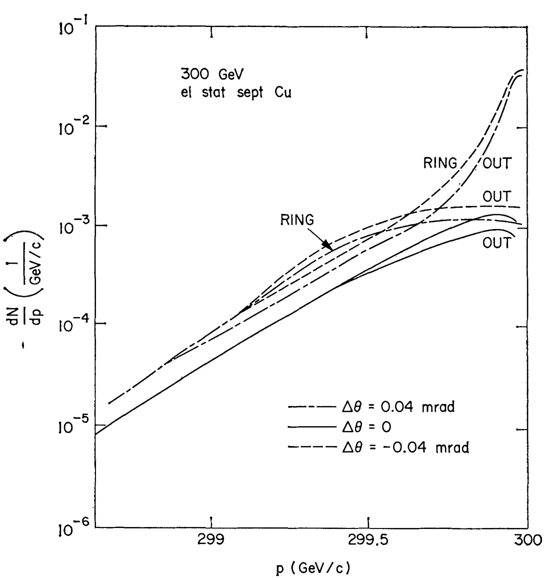

FIG. 3. Momentum distributions of scattered protons dN/dp from an electrostatic septum of the 300 GeV accelerator. All primary protons were assumed to have the momentum p_0. Separate curves are given for three different septum alignments $\Delta\theta$ and for protons scattered into the main ring and scattered out into the ejection channel.

3.2.2. *Scattering in Beam Scrapers.* The fate of protons hitting an absorber (beam scraper) at small angles can be studied with similar techniques.[108] We calculate the fractions of protons absorbed, F_a and scattered F_{sc}, for different materials and proton momenta as function of the angle of incidence. Such calculations can also be performed for absorbers made from magnetized iron. Table 3.V gives results for the case that the protons hit only the face of the scraper at small angles. Such calculations are of use to estimate the efficiency of scrapers which are supposed to remove protons arriving randomly by a mechanism that increases the betatron oscillation amplitudes slowly or shifts the closed orbit slowly.

TABLE 3.V
The absorbed fraction F_a (per cent) of protons hitting an absorber with angles between θ_1 and θ_2

		θ_1–θ_2 (mrad)				
p_0 (GeV/c)	Material	0–0.2	0.2–0.4	1.4–1.6	2.9–3.1	5–5.2
20	Be	59	84	95.5	97.5	99
20	Ti	32	50	90	96.5	99
20	Cu	37	55	87	96	99
20	W	38	46	72	89	97
20	Fe,B = 0	36				
20	Fe, B = 5 kG	50				
20	Fe, B = 10 kG	59				
20	Fe, B = 20 kG	73				
		θ_1–θ_2 (mrad)				
		0 –0.02	0.02 –0.04	0.14 –0.16	0.29 –0.31	0.5 –0.52
300	Be	73	87	95	98	99
300	Ti	44	67	93	97.5	99
300	Cu	44	66	94	98	99
300	W	39	54	87	95	99
300	Fe, B = 0 kG	44				
300	Fe, B = 2 kG	47				
300	Fe, B = 5 kG	53				
300	Fe, B = 10 kG	64				
300	Fe, B = 20 kG	77				

The fractions of scattered protons are rather high and increase with the atomic weight of the absorber material. The reasons for this behaviour are (i) the multiple Coulomb scattering angles increase strongly with atomic weight and (ii) the ratio of elastic-to-absorption cross section increases with atomic weight. It is a different problem to estimate the efficiency of a scraper used to remove multiple scattered protons at say $\lambda/2$ downstream from the septum where the radial density distribution of the protons is approximately known. Two situations for which calculations at 250 GeV were performed[105] are illustrated in Fig. 4. The proton beam is again assumed to have a divergence

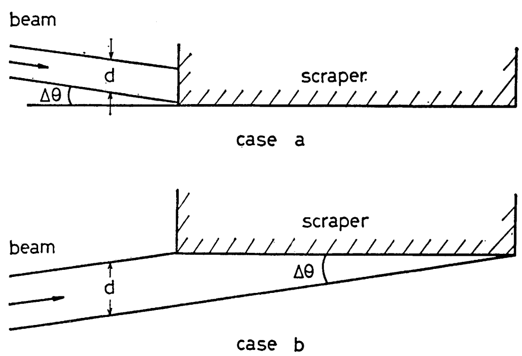

FIG. 4. A proton beam hitting a scraper, the two cases considered in the calculation.

spread $\Delta\theta = \pm 0.01$ mrad. Results are given in Table 3.VI. The outscattered fraction is in nearly all cases reasonably small. Therefore it is possible to construct beam scrapers with efficiencies on the order of 90 per cent.

TABLE 3.VI
Scattering of 250 GeV/c protons in scrapers. Results of Monte Carlo calculations for different materials and misalignments. The cases *a* and *b* are described in Fig. 4

Case	Misalignment $\Delta\theta$ (mrad)	Beam width d (cm)	Fraction of protons scattered out F_{sc}(%) Be	Fe	W
a	0	0.02	5	5.8	6.3
a	−1	0.02	0.15	0.06	0.11
a	0.1	0.02	19.9	10.4	8.5
a	1	0.2	18.6	8.8	5.5
b	−0.01	0.003	43.7	58.4	65.9
b	−0.1	0.03	16.5	18.6	30.8
b	−1	0.3	13	5.4	3.1

3.2.3. *Beam Loss Distributions in Proton Synchrotrons.* The calculation of beam loss distributions was reported in Refs. 109 and 110. Three kinds of beam losses are considered in synchrotrons: secondary particles produced in targets, ejection septa and beam scrapers; protons scattered out of targets, septa and scrapers, and true random beam losses all around the ring (like the beam loss due to gas scattering).

Calculations have been made for loss distributions due to secondaries and scattered protons from targets, septa and scrapers. The particle orbits in the accelerators are followed in the unperturbed lattices by matrix multiplications as in Ref. 111.

Calculations have also been done for the loss distributions using the ideal and unperturbed lattices. For a more detailed study of a working or proposed accelerator, field perturbations (quadrupoles, sextupoles, field bumps) used to excite the resonance employed for the ejection system could easily be taken into account. The influence of unwanted closed orbit distortions excited by magnet errors on the loss distributions should not be very strong along the first, say, 150 m (for 200 or 300 GeV accelerators) after the septum. Losses further away are probably mainly determined by the actual closed orbit deformations but such losses should be prevented by the use of beam scrapers.

The effect of secondaries, lost on the chamber walls, is for shielding purposes, proportional to their momentum. The secondaries are therefore weighted by the ratio P_{sec}/p_0.

Various loss distributions are given as follows:

(a) Figures 5 and 6 for the CERN PS downstream from an internal target which agrees well with measurements.[4]
(b) Figure 7 from secondaries downstream from an electrostatic foil septum in the 300 GeV accelerator with a SF lattice described in Ref. 112.
(c) Figure 8 after the same septum due to scattered protons.

Table 3.VII shows fractions of the circulating beam expected to be absorbed in septa and scattered into the main ring, the percentages P_{rev} and $P_{(150)}$ of scattered protons lost within the first revolution and the first 150 m after the septa and the distances after which 100 per cent (S_{100}) and 90 per cent (S_{90}) of the secondaries have reached the wall.

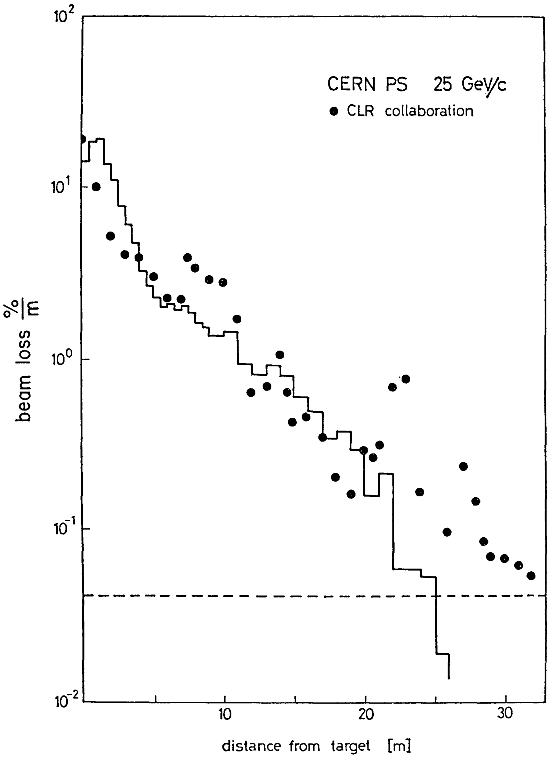

FIG. 5. Comparison of the calculated loss distribution in the first 30 m after an internal target in the CERN PS with measurements (Ref. 35).

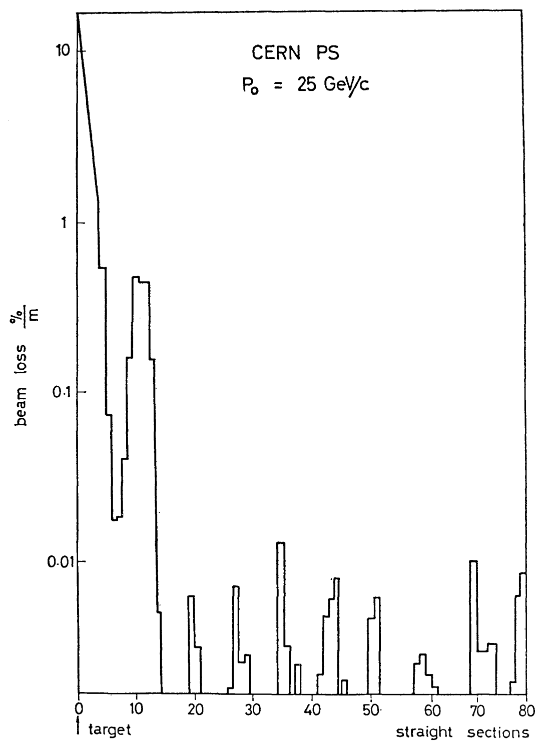

FIG. 6. Calculated loss distributions after an internal target in the CPS. Loss maxima occur each $(n+\frac{1}{2})\lambda/2$ after the target. A similar pattern is observed experimentally (see Ref. 35).

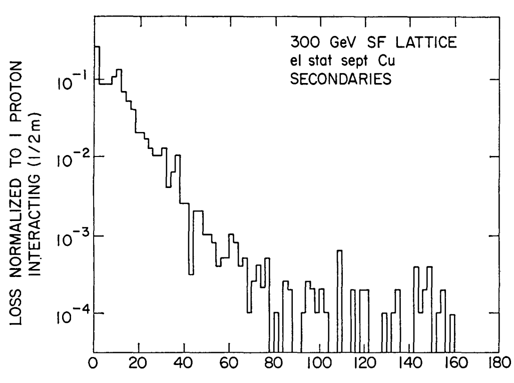

FIG. 7. Calculated loss distribution of secondaries after an electrostatic foil septum of the 300 GeV accelerator.

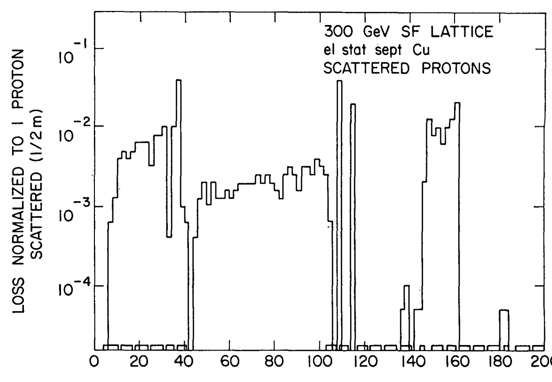

FIG. 8. Calculated loss distribution of scattered protons after an electrostatic septum of the 300 GeV accelerator with SF lattice.

TABLE 3.VII
Fractions of circulating beam absorbed (F_a) in septa and fractions scattered back into main ring (F_r). Distances after which 100 per cent (S_{100}) and 90 per cent (S_{90}) of the secondaries have reached the wall. Percentage of scattered protons lost within the first revolution (P_{rev}) and within 150 m after the septa (P_{105})

	Septum lens 63 of the CERN PS	Electrostatic septum 300 GeV accelerator	Wire septum 250 GeV
F_a [% of circulat. beam]	1.5	0.5	0.1–0.3
F_r [% of circulat. beam]	1	0.3	0.3–1.5
S_{100} (m)	32	163	160
S_{90} (m)	4	25	25
P_{rev} [%]	81	64	—
P_{150} [%]	79	50	—

3.3. *The Monte Carlo Calculation of the Hadronic Cascade*

The nucleon–meson cascade is a phenomenon which is far too complicated to be calculated without drastic simplification and approximations. In principle, all long and short lived elementary particles are involved and they interact by strong, electromagnetic, and weak interactions. To give a complete description of the cascade, we would need a complete knowledge and understanding of all phenomena in high energy physics.

The dominant features of the nucleon–meson cascade can however be understood with much less information about the particles and their interactions.

Among the particles which interact strongly with the nuclei in the shielding material, it is sufficient to regard only protons, neutrons and pions, because only these appear in significant numbers. Experimental results indicate that K mesons are produced by a factor of about 10 less frequently than pions. They can therefore be neglected relative to the π mesons. Hyperons and antinucleons are produced in small numbers compared to the number of protons and neutrons, therefore they can be neglected as well.

Electron–photon showers are initiated in great numbers by the decay of neutral, mainly π^0, mesons. However, since in usual shielding materials the radiation length is much shorter than the absorption length for strongly interacting particles, these electron–photon cascades die out relatively fast and play only a minor role for the energy transport of the cascade. They are, however, very important for the energy deposition.

Muons, which are produced by the decay of π and K mesons, have no strong interaction. They can only be stopped by ionization energy losses in the shielding material, therefore they represent a very penetrating component of the cascade which cannot be neglected. At energies higher than about 100 GeV/c energy losses due to bremsstrahlung, pair creation and nuclear interactions become also important[145,146] and should be taken into account.

The proton, neutron, pion and muon components of the cascade are treated separately where the muons are produced by the decay of π and K mesons restricting ourselves, however, to particles with energies above a certain cut-off energy, usually $E = 100$ MeV, and do not consider any secondary particle production with energies below $E = 125$ MeV. Therefore we have to consider mainly the high energy interactions of particles with nuclei and can ignore most of the nuclear processes which dominate at lower energies. Not considered separately are most of the low energetic particles resulting from the intranuclear cascade and from nuclear evaporation. These processes are only mentioned roughly when calculating the energy deposited in the material. Neutrons below 10 to 15 MeV form the most abundant component of the cascade which play, however, no large role for the energy transport. We believe that a knowledge of the density of high momentum particles in the cascade is necessary to understand the behaviour of this low energy neutron component, too.

Apart from particle production processes in the high energy inelastic collisions, multiple Coulomb scattering and ionization energy loss of the charged particles are considered in the calculation as well as the elastic scattering and the decay of π and K mesons into muons.

The production of protons and neutrons in high energy collisions is treated on an equal footing, however, detailed experimental information exists only for proton production. The proton and neutron densities in the shield become, however, quite different because of the ionization energy losses from the protons.

For a complete description of the cascade it would be necessary to calculate the density functions of the tracks or stars (nuclear interactions) produced by all kinds of particles involved inside the shielding material. These density functions are very complicated and depend on many variables. The density of particles of kind i would be described completely by the function

$$\varphi_i(p, x, y, z, \cos\theta_x, \cos\theta_y, \cos\theta_z) \tag{3.1}$$

where x, y and z are here the co-ordinates of the given volume element in the shielding material, p is the momentum of the particle and $\cos\theta_x$, $\cos\theta_y$, and $\cos\theta_z$ are the direction cosines, which describe the direction of flight of the particles.

For any three direction cosines the restriction holds:

$$\cos^2\theta_x+\cos^2\theta_y+\cos^2\theta_z = 1. \tag{3.2}$$

In the case of the star densities, p and the direction cosines refer to the interacting particle. There are far too many variables for a function which is to be calculated by a Monte Carlo method. The calculation time necessary to obtain a sufficient statistical accuracy would be too long with present-day computers.

If we calculate the cascade initiated by a narrow proton beam impinging on the shielding material it is justified to assume cylindrical symmetry of the particle densities around the direction of the incident beam. Therefore we get a complete description of the cascade by

$$\varphi_i(p, r, z, \cos\theta_x, \cos\theta_y, \cos\theta_z). \tag{3.3}$$

There are still too many variables in expression (3.3). For sufficient statistical accuracy we must always integrate function (3.3) over some of the variables.

In the following the density functions are given which are actually calculated:

(i) The three-dimensional star or track density as function of the longitudinal depth in the shield z and the distance from the beam axis r

$$F_i(r, z) = \iiint d\cos\theta_x\, d\cos\theta_y\, d\cos\theta_z \cdot \delta(\cos^2\theta_x+\cos^2\theta_y+\cos^2\theta_z-1) \cdot \int_{p_c}^{p_0} \varphi_i(p, r, z, \cos\theta_x, \cos\theta_y, \cos\theta_z)\,\mathrm{d}p. \tag{3.4}$$

p_c is the cut-off momentum and p_0 is the momentum of the incident protons. The integral over the three direction cosines has the limits $-1 \leqq \cos\theta_i \leqq 1$. The δ-function is used to fulfil the condition

$$\cos^2\theta_x+\cos^2\theta_y+\cos^2\theta_z = 1.$$

(ii) The laterally or longitudinally integrated star or track densities which are obtained by integrating Eq. (3.4) further over r or z.

$$F_{zi}(z) = \int_0^\infty 2\pi r F_i(r, z)\,\mathrm{d}r, \tag{3.5}$$

$$F_{ri}(r) = \int_0^\infty F_i(r, z)\,\mathrm{d}z. \tag{3.6}$$

The laterally or longitudinally integrated star or track densities are of importance if one wants to estimate the shielding requirements for situations which differ from the situation considered originally in the calculation. We consider the calculation of the star densities resulting from a narrow incident proton beam in an end stop. The laterally integrated star density gives then just the longitudinal star density $F(z)$ in the case of a very wide incident beam of uniform density. The longitudinally integrated star density gives the radial dependence of the star density $F(r)$ in the case of a uniform line source along the centre of a cylinder—a situation which might be of use to estimate the radiation problems caused by the interaction of protons along the vacuum chamber inside magnets of a synchrotron or beam line.

These distributions are calculated for protons, neutrons, pions and muons separately as well as for all strongly interacting particles together.

The π mesons are treated separately in the calculation and K mesons are expected to be produced by a factor of 10 less frequently than pions. Therefore the K meson fluxes will not contribute essentially to the track or star density in the shielding material. If muon fluxes are of interest, however, we cannot neglect the decay of K mesons because of their shorter lifetime as compared to pions. With respect to the decay, 10 per cent of the pions in our calculation are taken into account as kaons.

The lifetimes of π and K mesons in their rest systems are

$$t_\pi{}^* = 2.55\times10^{-8}\,\mathrm{s}, \quad t_K = 1.224\times10^{-8}\,\mathrm{s}. \tag{3.7}$$

The decay $K \to \mu + \nu$ has a branching ratio of 63.1 per cent, so we use the partial lifetime

$$t_K{}^* = 1.94 \times 10^{-8}\,\text{s}. \tag{3.8}$$

From this the decay length is

$$\begin{aligned} \lambda_\pi &= (p/m_\pi)ct_\pi{}^* = (p/m_\pi)765\rho\ [\text{g/cm}^2], \\ \lambda_K &= (p/m_K)ct_K{}^* = (p/m_K)582\rho\ [\text{g/cm}^2]. \end{aligned} \tag{3.9}$$

ρ is the density of the shielding material, p is the pion or kaon momentum in GeV/c and m_π and m_K are the masses in GeV/c^2.

From the decay length we estimate that about one pion or kaon in approximately 100 to 1000 will decay. For sufficient statistical accuracy for the muon densities, the decay probabilities must be increased for pions and kaons.

The probability to decay in the interval between x and $x+\mathrm{d}x$ for a particle starting its path at $x = 0$ is

$$\lambda^{-1} \exp(-x\lambda^{-1})\,\mathrm{d}x. \tag{3.10}$$

In our calculation we increase this by a factor 500. Particles which are not stopped by nuclear interactions would with this increased decay probability decay just 500 times. Therefore the resulting muon flux must be given a weight factor of 0.002.

The Monte Carlo nucleon–meson cascade calculation takes only particles into account with energies above a certain threshold energy E_{thr}, with typical values between 50 and 125 MeV. This is sufficient to calculate star and track densities for shielding purposes since the energy in the cascade is mainly transported by particles with higher energy. For the calculation of the energy deposition it would however be advantageous to consider also particles with lower energy. All the energies of these particles (low energy cascade and evaporation) have to be added to the nuclear excitation energy, which is not sufficiently well known. This is the main difficulty in the calculation of the energy deposition.

We calculate the distribution of energy density deposited

$$\phi_E(z, r)\ [\text{GeV/cm}^3 \text{ per incoming primary particles}] \tag{3.11}$$

inside a cylindrical block of material. The primary particles of momentum p_0 in a well collimated beam in z direction hit the block at $z = 0$ and $r = 0$. The energies deposited by the cascade particles are collected into a histogram representing $\phi(z, r)$. We assume that all energy deposited appears finally in the form of ionization or excitation of the atoms in the material contributing to the heating of the material, scintillation yields, radiation damage, etc.

The following contributions to the energy deposition are taken into account:

(i) The ionization energy loss of all charged primary and secondary particles considered is distributed along their paths. This contribution is straightforward to calculate.

(ii) Secondary particles created with energies below E_{thr} are assumed to stop immediately. All the energy of these particles is deposited within the bin where the particle was created. This is certainly a very crude approximation (see the discussion later under point iv). This contribution is only of minor importance.

(iii) Neutral π mesons are not usually regarded in the cascade calculation. They decay rapidly and do not contribute much to the energy transport in the cascade because the radiation lengths are in most materials much shorter than the absorption lengths of strong interacting particles. The electromagnetic cascades induced by decaying π^0 mesons are, however, a very efficient mechanism to deposit the energy in the form of ionization. It is assumed that the energy and angular spectra of secondary π^0 mesons are the same as the experimentally well known π^+ spectra. The computer programme creates π^0 mesons randomly in the same way as charged pions. The decay of the π^0 meson is treated approximately in the calculation. The spatial distribution of the energy deposited by the electromagnetic cascade has been studied extensively both experimentally and theoretically. We distribute the energy of the decay according to longitudinal and transverse energy distributions obtained by interpolation and extrapolation from curves measured or calculated. (See Sec. 2.5.)

(iv) The most uncertain contribution comes from nuclear processes. In collisions with nuclei other than hydrogen not all the energy of the primary particles is used to create high energy secondaries. A certain amount of the energy E_{ex} is used to excite the nucleus. Some nucleons or nuclear fragments are knocked out by the intranuclear cascade, another part of E_{ex} is used to evaporate protons and neutrons from the nucleus. The excited nucleus may need some time before it decays into a stable one. According to the evidence from spallation investigations medium heavy target nuclei like Fe or Cu may lose in this way about 15 nucleons per interaction with protons or neutrons of some GeV energy.[140] Intranuclear cascade calculations[121] lead to approximately the same results, these calculations are, however, only available for rather low primary energies.

The excitation energy E_{ex} depends on the energy E of the primary particle and on the kind of target nucleus (atomic weight A). At low energy, below the threshold energy E_{thr} in the cascade calculation, we assume $E_{ex} = E$. For $E > E_{ex}$ we use the ollowing crude formula

$$E_{ex} = A/100\,[\mathrm{GeV}] \quad \text{for} \quad E > 3\text{ GeV} \qquad (3.12)$$

$$E_{ex} = E_{thr} + \frac{(E-E_{thr})(B-E_{thr})}{(3-E_{thr})} \quad \text{for} \quad E_{thr} \leqq E \leqq 3\text{ GeV}$$

B is the larger one of E_{thr} and $A/100$.

Only one third of this excitation energy is assumed to be deposited within the bin where the interaction occurs. Two thirds of E_{ex} is assumed to be carried away by low energetic neutrons and is deposited isotropically around the position of the star according to an exponential $r^{-2} \cdot \exp(-r/\lambda_{abs})$. r is the distance from the positions of the star and λ_{abs} is the interaction length of 50 MeV neutrons.

It is clear that this crude approximation for the magnitude of the excitation energies and their deposition in the material can only lead to very approximate results and efforts are needed to improve this situation. The importance of this term decreases, however, with increasing primary energy and the fraction of the energy deposited via electromagnetic cascades from π^0 decay increases with primary energy.

Two different Monte Carlo methods for the calculation of the hadronic cascade are used. The first, described in Refs. 31–37 and 39 is used in the computer programmes TRANSK (and KASTRA). The second one described in Refs. 38, 40–42, 44 and 45 is used in the programmes FLUTRA, MAGTRA and TASTAK which differ only in the geometry of the shielding material. The main difference of the two methods is the treatment of energy conservation in single scattering events.

Two of the requirements in the Monte Carlo calculation are the following: the secondary particles used in the calculation should be distributed in momentum and angle according to the known secondary particle spectra. Energy should be conserved in the scattering events. In TRANSK we select randomly secondary particles from the given distribution functions and use these particles sacrificing energy conservation in single events but conserving the energy in an average sense for each group of scattering events with equal primary particle and the primary momentum within given intervals. Only average properties of the cascade can be calculated with such a method like star and track densities, energy spectra of the particles, or the distribution of energy deposited in the material.

In cases where a great number of particle histories are considered, this procedure does not lead to any errors. For cascades initiated by particles of very high primary energy only a small number of primary particles can be followed in a finite computer time. In such cases errors in the normalization of the computed distributions might result from this method in TRANSK.

The method applied by FLUTRA differs. The energy in each single event is conserved. The original aim of FLUTRA was to calculate properties of cascades excited by single primaries. This can be done without excessive expense of computer time and memory space. We select as before secondaries randomly from the given distribution functions. In each collision considered there is a situation where the next selected secondary particle has too large an energy which would violate the energy conservation. This particle is stored, to be used later, and instead a particle with just the missing energy is used which becomes the last secondary created in the event considered. The kind of this last particle has also to be selected randomly and the inelasticities for the creation of secondaries must on the average also be correctly fulfilled. These last arbitrarily created particles would deform the spectra of secondary particle creation and therefore the parameters of these particles are stored. If later a similar secondary particle is created from the distribution functions, it will be thrown away. The method satisfies thus both the secondary particle spectra and energy conservation for each event.

In both calculations the inelasticities

$$K_{ij}^0 = 1/E_i \int E_j \frac{d^2N}{\mathrm{d}p\,\mathrm{d}\Omega}\,\mathrm{d}p\,\mathrm{d}\Omega \qquad (3.13)$$

determine the fraction of primary energy carried away by each kind of secondary particle. Table 3.VIII lists the inelasticities K_{ij}. The sum of the values K_{ij}^0 in Table 3.VIII is one. The values given

TABLE 3.VIII
Inelasticities K_{ij}^0 used in the cascade calculation

Incoming particle	Outgoing particle p	n	$\pi^\pm$	π^0
p	0.3	0.3	0.25	0.15
n	0.3	0.3	0.25	0.15
$\pi^\pm$	0.2	0.2	0.4	0.2

for incident protons and neutrons agree with measured particle spectra at primary energies between 10 and 30 GeV and with cosmic ray experiments. No energy dependence is assumed since sufficient data are not available. Hyperons and kaons are not treated separately but are included in the nucleon and pion components, respectively. A certain part of the energy is however used for nuclear excitation E_{ex}, which depends on the particle energy and the atomic weight of the target.

The inelasticities are therefore corrected in the following way:

$$K_{ij} = K_{ij}^0\left(1-\frac{E_{ex}}{E_0}\right). \qquad (3.14)$$

Another difference in the methods is the use of particle splitting techniques and similar methods, which are used in TRANSK but not in FLUTRA. If the properties of the cascade at very large depths in longitudinal or transverse direction are of interest, it is advisable to use TRANSK. If the core of the cascade is of interest, FLUTRA is the better programme.

The programmes calculate first integrals of the particle yield formulae $d^2N/\mathrm{d}p\,\mathrm{d}\Omega$ which are needed for the random selection of secondary particles. To select randomly the momentum p of a secondary particle, which is produced by a primary particle of momentum p_0 we must first normalize the functions $\mathrm{d}n/\mathrm{d}p$ to unity

$$F(p, p_0) = \{\mathrm{d}N(p_0)/\mathrm{d}p\}\Big/\int_0^{p_0} \{\mathrm{d}N(p_0)/\mathrm{d}p\}\,\mathrm{d}p. \quad (3.15)$$

With the help of a random number x, equally distributed between 0 and 1, we can then determine a random p_x

$$x = \int_0^{p_x} F(p, p_0)\,\mathrm{d}p. \qquad (3.16)$$

Solving (16) for p_x gives

$$p_x = \phi(x, p_0). \qquad (3.17)$$

The computer calculates and stores the functions $\phi(x, p_0)$ for x values between 0 and 1, and for p_0 values needed. Using these stored values, the selection of random momenta can be done very efficiently in the computer by selecting one random number and performing one interpolation. Next we calculate (only in TRANSK) the density of stars which are produced by the primary protons inside the shielding material.

We assume a well collimated beam of primary protons of momentum p_0 and with a given cross section. In a Monte Carlo calculation the fate of each single proton is followed in this beam. The probability for nuclear interaction of the protons inside the shield is a well-known function of the path length in the shielding material. The nuclear interactions therefore change only the weight factors of the protons. Elastic and multiple Coulomb scattering of the protons are, however, determined using random numbers.

The result of this Monte Carlo calculation is the three-dimensional density distribution of primary proton stars inside the shielding material.

In the following central part of the computer programmes we calculate the densities of protons, neutrons, pions and muons inside the shield, which are produced by the inelastic interaction of one primary proton at the depth $z = 0$ in the shielding material in the case of TRANSK. The same is done with an additional selection of the point of interaction of the primary particle in FLUTRA. Another point of difference is the particle splitting applied only in TRANSK and energy conservation in each scattering event applied only in FLUTRA. A simplified flow diagram of this routine DISEK (belonging to TRANSK) is given in Fig. 9.

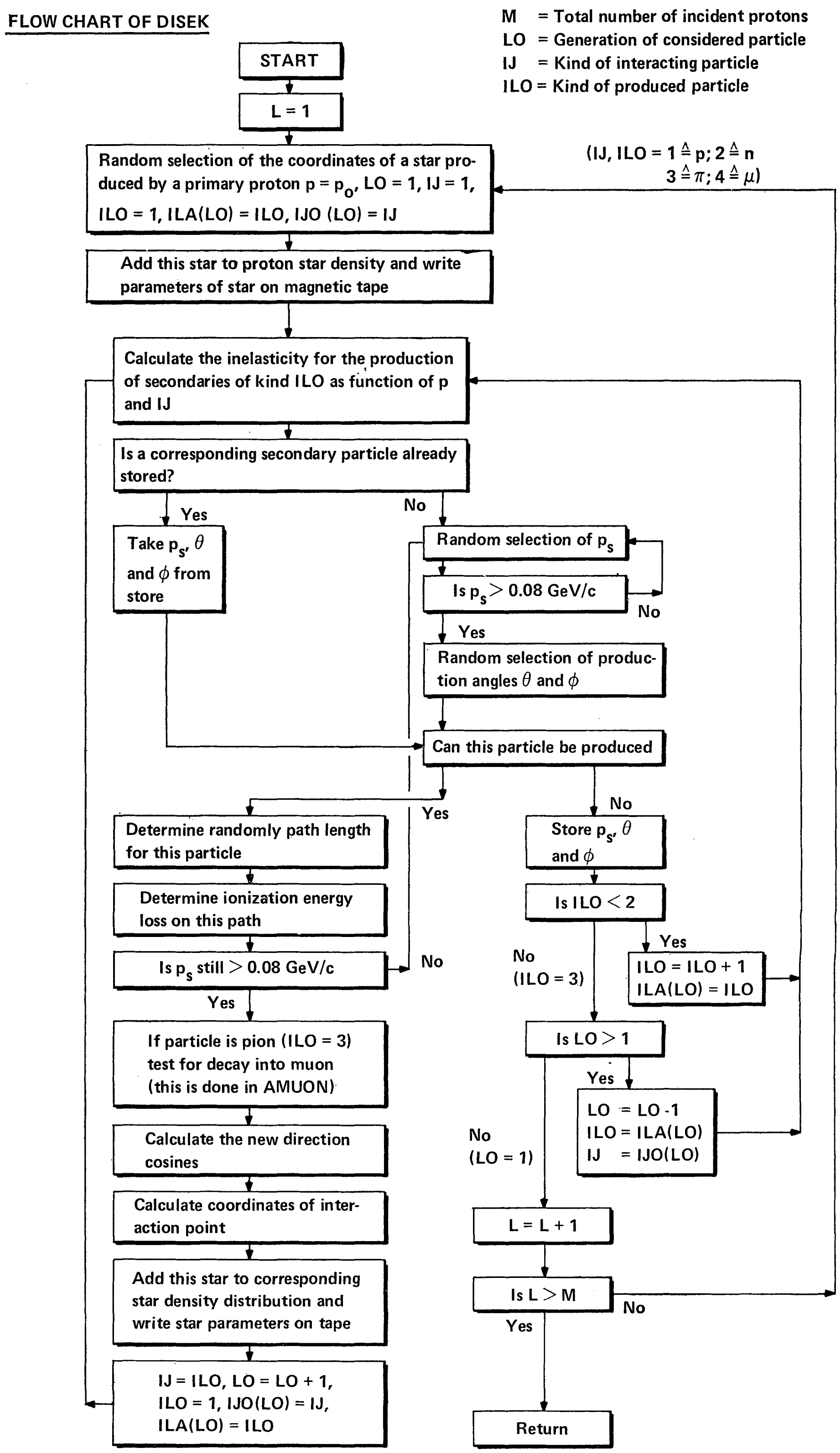

FIG. 9. Flow diagram of the computer routine DISEK of the programme TRANSK.

The secondary particles of all kinds, which are produced by the primary and in all following nuclear interactions, are selected randomly from the corresponding distribution functions for momentum and angle.

First we select p randomly using the tabulated function (3.17). The angle θ is selected randomly from the distribution functions (2.12) or (2.13) for the given p_0 and the already selected p. The function $\phi(x, p_0, p)$ corresponding to (3.17) can in most cases be determined analytically. Finally, we select randomly the angle φ from a uniform distribution between 0 and 2π.

Pions and kaons decay into muons according to the exact decay kinematics. The distance which the particles travel inside the shield is selected randomly using the corresponding nuclear mean free path. Ionization energy losses on this path are correctly taken into account. Particles disappear in the calculation only by absorption or when they are stopped by ionization energy losses to less than the cut-off momentum p_c. Finally FLUTRA normalizes, prints, and plots the wanted distributions.

In TRANSK we have still to combine the star density of primary protons and the secondary star density for primary protons interacting at one point before obtaining the final results.

FLUTRA calculates the star densities for p, n, π, and all the strong interacting particles as well as the density of energy deposition. It also gives a histogram of the total energy deposited by single protons in blocks of different sizes (TANC Total Absorption Nuclear Cascade detector or SANC Sampling Total absorption detectors) (see Refs. 123–127).

TRANSK calculates the star densities, muon track densities, the density of energy deposition, energy, and angular distributions of the cascade particles as a function of the depths z or the distance r defined as follows:

The energy spectrum of the particle i as function of the depth z of the cascade is

$$F_{pi}(E, z) = \iiint d\cos\theta_x, d\cos\theta_y, d\cos\theta_z \cdot \delta(\cos^2\theta_x + \cos^2\theta_y + \cos^2\theta_z - 1). \quad (3.18) \cdot \int_0^\infty 2\pi r \varphi_i(E, r, z, \cos\theta_x, \cos\theta_y, \cos\theta_z)\,\mathrm{d}r$$

The angular distribution of particles i as function of the depth z of the cascade is

$$F_{\theta_i}(\cos\theta_z, z) = \iint d\cos\theta_x, d\cos\theta_y, \cdot \delta(\cos^2\theta_x + \cos^2\theta_y + \cos^2\theta_z - 1) \cdot \int_0^\infty 2\pi r\,\mathrm{d}r \quad (3.19) \cdot \int_{p_c}^{p_0} (p, r, z, \cos\theta_x, \cos\theta_y, \cos\theta_z)\,\mathrm{d}p.$$

The Monte Carlo cascade calculations are performed for a variety of geometrical arrangements which resemble closely situations around an accelerator, for example:

TRANSK and FLUTRA—a massive cylinder[29–35,37,39,40,44] which represents either an end-stop or a target,

MAGTRA—a target in front of or inside a hollow cylinder[38,41–43] representing a target in front of a magnet unit or a target or beam stopper inside an empty tunnel,

TASTAK—a target in front of a sandwich magnet or collimator,[45]

KASTRA—a line source, representing the target and vacuum tube, and some magnet units inside a cylindrical tunnel.[7,36]

4. RESULTS OF MONTE CARLO CASCADE CALCULATIONS AND COMPARISON WITH EXPERIMENTAL DATA

4.1. *Comparison with Emulsion Experiments*

The three-dimensional development of the hadronic cascade star and track densities has been measured in a number of emulsion experiments around high energy accelerators, mainly the CERN PS.[1,2] Steel and concrete were mainly used as shielding material. Well collimated incident proton beams with momenta between 6 and 24 GeV/c collided with a large backstop of the material considered. The measurements[1] at $p_0 = 19.2$ GeV/c are compared with the results of the calculation in Figs. 10–13. All curves are normalized to unit proton star or track density at $z = 0$ and $r = 0$. The laterally integrated densities in Fig. 12 and the densities along and outside the beam axis

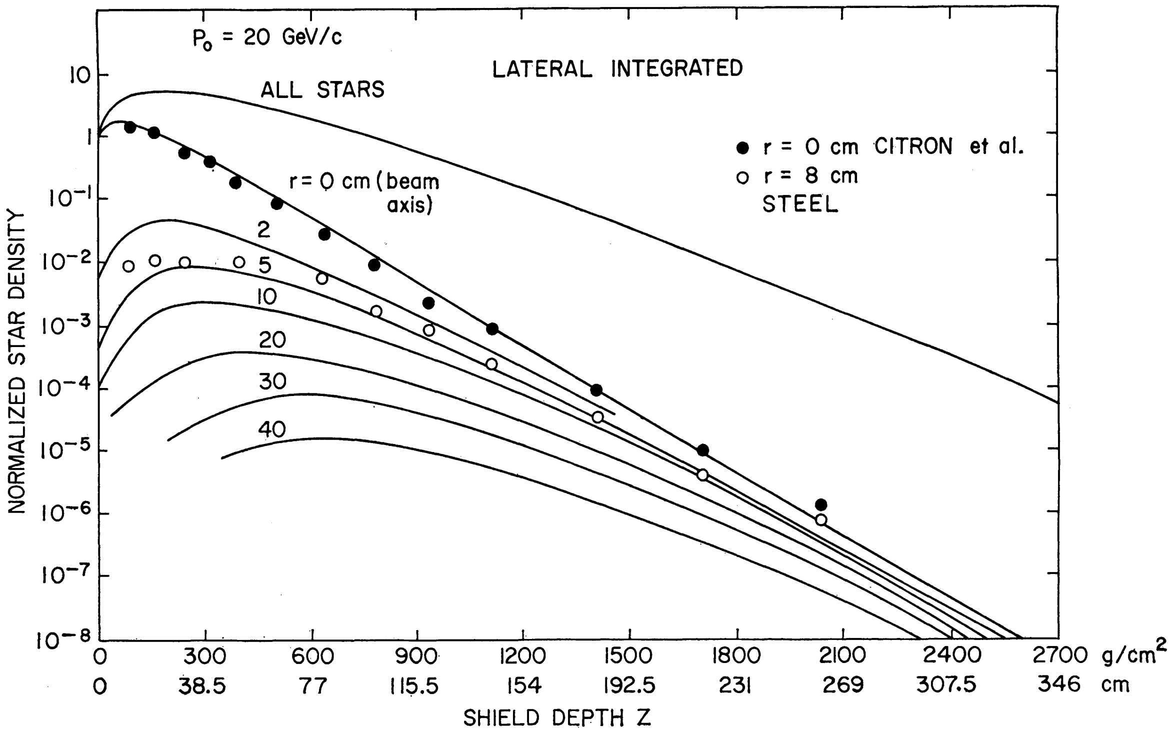

FIG. 10. The longitudinal development of the total star density (sum of proton, neutron and pion star densities) for a cascade initiated by a well collimated proton beam of cross section $10 \times 10\,\text{mm}^2$ and momentum $p_0 = 20$ GeV/c in steel. The curves are normalized to unit proton star density at $r = 0$. The points represent the star densities along the beam axis ($r = 0$) and 8 cm outside the beam axis ($r = 8$ cm) which were measured by Citron *et al.*[1]

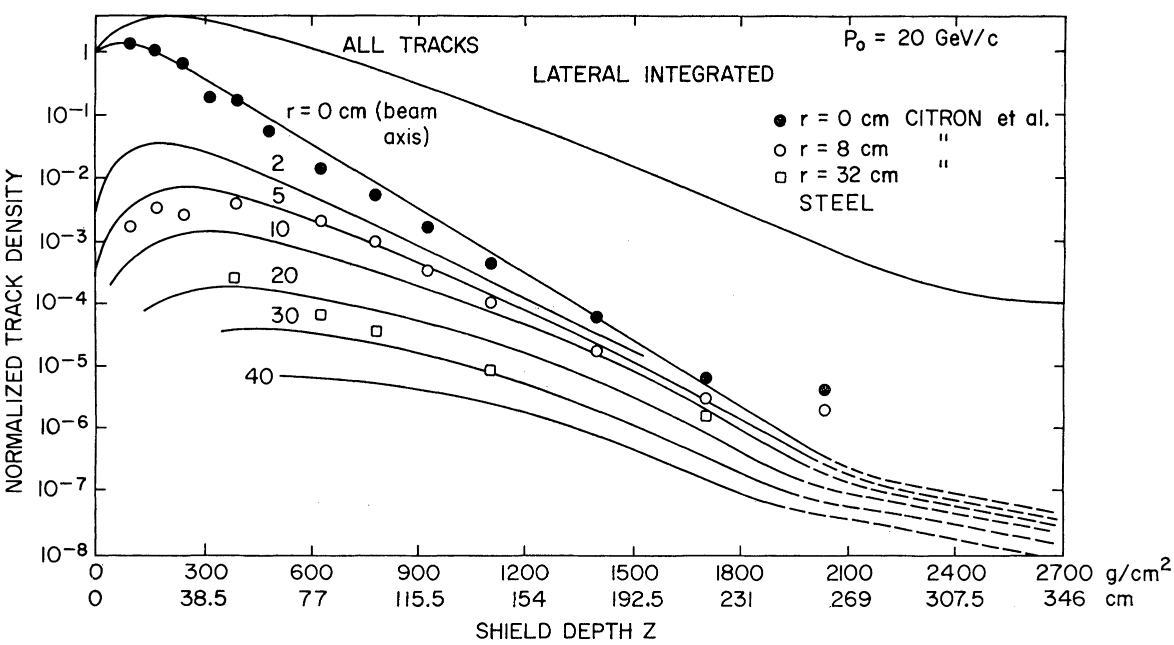

FIG. 11. The longitudinal development of the total track density (sum of proton, pion and muon track densities) for a cascade initiated by a well collimated proton beam of cross section $10 \times 10\,\text{mm}^2$ and momentum $p_0 = 20$ GeV/c in steel. The curves are normalized to unit proton track density at $r = 0$ and $z = 0$. The points represent the track densities along the beam axis ($r = 0$ cm) and 8 and 32 cm outside the beam axis ($r = 8$, 32 cm), which were measured by Citron *et al.*[1] The change in the slope of the curves near the depth $z = 2000\,\text{g/cm}^2$ arises from the muon track density.

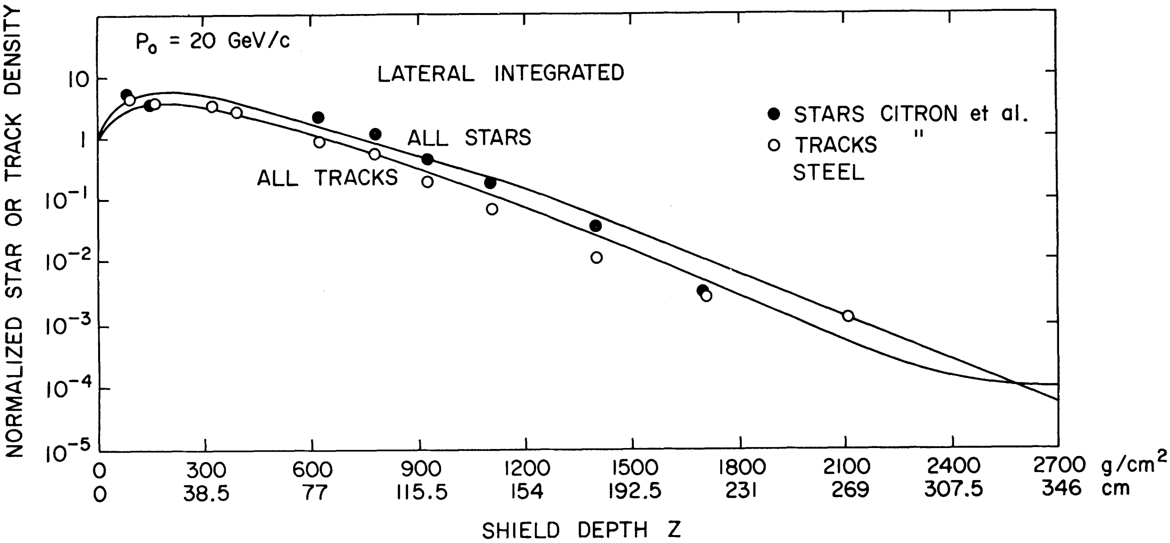

FIG. 12. Lateral integrated total star density and total track density for a cascade initiated by a well collimated proton beam of momentum $p_0 = 20$ GeV/c in steel. The points given represent the experimental integrated track and star densities which were given by Citron *et al.*[1]

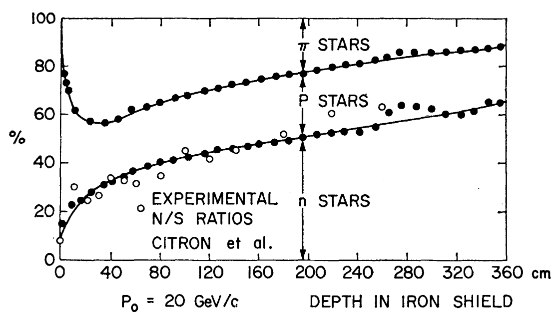

FIG. 13. Percentage of neutron, proton and pion stars contributing to the total star density of a cascade initiated by a proton beam of $p_0 = 20$ GeV/c as function of the depth z in the shield. At $z = 0$ nearly 100 per cent of the stars are proton stars. The fraction of pion stars reaches a maximum of 45 per cent at $z = 30$ cm and decreases with z. The fraction of neutron stars increase steadily and reaches 60 per cent at about $z = 300$ cm. The points give the percentage of stars without primary track in the backward hemisphere (N/S) as measured by Citron *et al.*[1] This represents a lower limit for the fraction of neutron stars.

in Figs. 10 and 11 agree very well with the corresponding experimental values. In Fig. 13 the percentage of neutrons, pions and protons obtained in the calculation is plotted as function of the depth z inside the shielding material. The agreement with the experimentally determined fraction of neutrons[1] is good. This plot shows that the relative importance of the neutron component increases with depth z.

All the star densities given are normalized to unit proton star density at $z = 0$ and $r = 0$. We get star densities normalized to one incoming proton in stars per cm^3 by multiplying the given curves by

$$[1-\exp(-p/\lambda p, \text{abs})] = 0.0614$$

$$\text{for Fe } [\lambda_{p,\text{abs}}(\text{Fe}) = 123 \text{ g/cm}^2]. \tag{4.1}$$

The track densities are normalized to unit proton track density at $r = 0$ and $z = 0$. Since the incoming proton beam has a cross section of 1×1 cm^2, the curves correspond to the track densities in tracks per cm^2 normalized to one incoming proton.

4.2. *Longitudinal and Transverse Development of the Cascade*

Figure 14 gives the calculated total star density plotted as function of the distance r from the beam axis in a large Fe backstop (different curves are given for different depths z in the shield).

The behaviour of track and star densities can be characterized by some parameters:

B is the build-up factor. The laterally integrated star or track densities decrease after a certain transition region approximately exponentially. By extrapolating this exponential decrease in backward direction to the depth $z = 0$, one finds the build-up factor B.

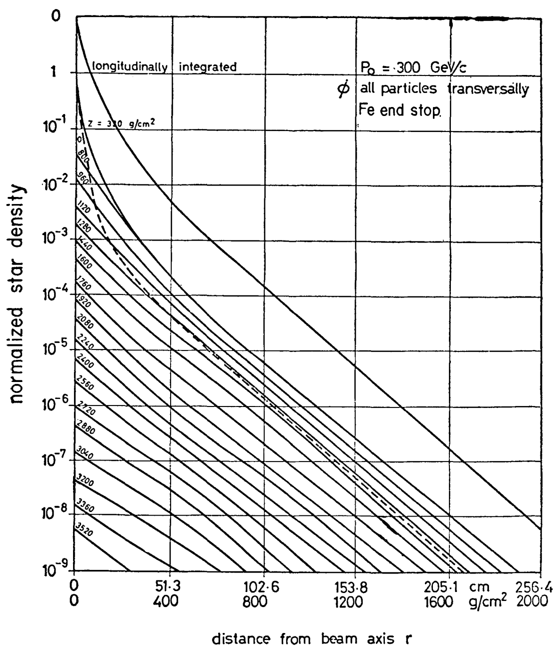

FIG. 14. Transverse development of the total star densities $\phi(r, z)$ and $\phi(r)$ in a Fe cylinder for an incoming proton beam of $p_0 = 20$ GeV/c.

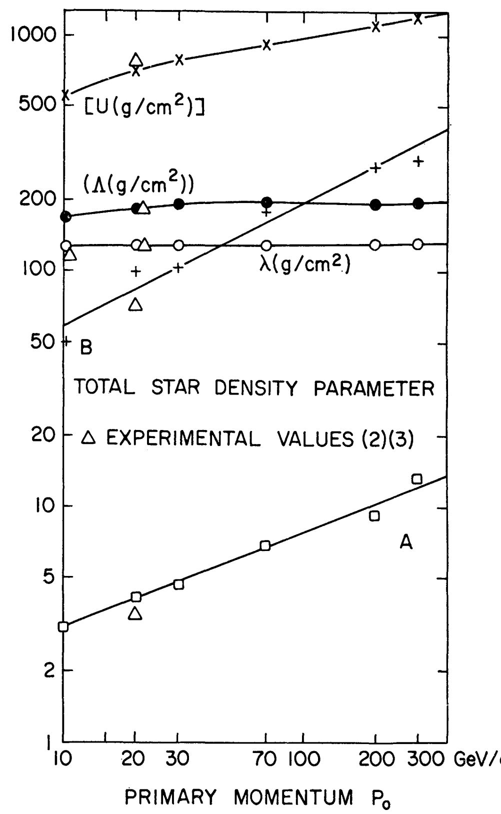

FIG. 15. The parameters B, Λ, A, U and λ characterizing the total star density as function of the primary momenta p_0. The experimental parameters for $p_0 = 10$ and 20 GeV/c are from Ref. 1.

Λ is the attenuation length, which determines the slope of the exponential decrease of the laterally integrated star or track density.

A is the maximum value reached by the laterally integrated track or star densities.

U is the depth at which the laterally integrated densities after the transition region reach again the value 1.

The integrated neutron or pion star densities may have maxima with $A < 1$, because of the normalization of all curves to unit proton star density at the depth $z = 0$. In this case we have no U value.

The star or track densities along the beam axis (at $r = 0$) decrease after the transition region approximately exponentially.

λ is the attenuation length, which determines the slope of this exponential decrease.

The calculated values for these parameters of the total star density are given in Fig. 15 together with experimental values (1.2) for 10 and 20 GeV/c.

The star densities multiplied with the distance r from the beam axis $r \cdot \Phi(r,z)$ and $r \cdot \Phi(r)$ decay exponentially for larger r values within the statistical errors:

$$r \cdot \Phi(r) \approx \exp(-r/\lambda_r). \tag{4.2}$$

In Table 4.I we give the transverse attenuation on length λ_r determined from the calculated $r \cdot \Phi(r)$ curves for neutrons, protons, pions, all particles (n, p, π) and all charged particles (p, π).

The transverse attenuation lengths λ_r are nearly independent on p_0 (possibly, they increase slightly with p_0). This results from the transverse momenta of the created particles being independent of p_0.

This conclusion fully justifies the use of the results of transverse shielding experiments at present accelerators for the design layout of shielding for future accelerators.

TABLE 4.I
Transverse attenuation length λ_r in g/cm² for the curves $r \cdot \Phi(r)$

p· [GeV/c]	Shield	n	p	π	n, p, π	p, π
20	Fe	136	131	129	136	130
70	Fe	134	121	115	130	118
300	Fe	140	129	119	133	123
20	Al	109	103	93	109	101
70	Al	114	108	103	113	106
300	Al	120	114	103	116	109

We see from the star density curves as well as from the transverse attenuation length λ_r, that the neutron component of the cascade is also the most important one in transverse direction.

The curves in Fig. 14 represent the star densities in stars/cm³. The particle fluxes (in particles per cm²) are assumed to be proportional to the star densities. A flux of one particle cm^{-2} corresponds to a star density of

$$1-\exp(-\rho/\lambda_{abs}) \quad [\text{stars}\cdot\text{cm}^{-3}] \qquad (4.3)$$

(for Fe this is 0.0614 stars cm^{-3}; ρ is the density of the material).

We may use the calculated densities to evaluate shielding dimensions and consider external proton beams of 20 and 300 GeV/c momentum.

Table 4.II gives longitudinal and transverse dimensions of backstops necessary to attenuate the

TABLE 4.II
Dimensions of backstops for external proton beams

	Beam intensity [p/s]	10^{11}	10^{12}	10^{13}	10^{14}
Fe	Longitudinal [g/cm²]	3100	3400	3700	4000
$p_0 =$	,, [cm]	400	435	475	510
20 GeV/c	Transverse [g/cm²]	2100	2400	2700	3000
	,, [cm]	270	310	345	385
Earth	Longitudinal [g/cm²]	2480	2720	2960	3200
$p_0 =$	,, [cm]	1380	1510	1650	1780
20 GeV/c	Transverse [g/cm²]	1680	1920	2160	2400
	,, [cm]	935	1070	1200	1330
Fe	Longitudinal [g/cm²]	4200	4600	5000	5400
$p_0 =$	,, [cm]	540	590	645	695
300 GeV/c	Transverse [g/cm²]	2350	2650	2950	3250
	,, [cm]	300	340	380	415
Earth	Longitudinal [g/cm²]	3360	3680	4000	4320
$p_0 =$	,, [cm]	1870	2040	2210	2390
300 GeV/c	Transverse [g/cm²]	1870	2110	2350	2590
	,, [cm]	1040	1170	1300	1440

fluxes down to the constant level of 4.3 high energy hadrons in equilibrium with low energy neutrons and produce, together with these low energy components, a dose of about 4.3 mrem/h.

4.3. *Energy Spectra of the Cascade Particles*

Figures 16 to 18 give calculated proton, neutron and pion energy spectra for different radii, r, in an

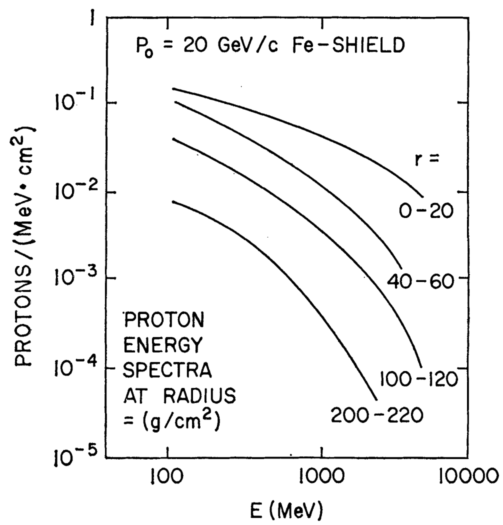

FIG. 16. Calculated proton energy spectra in a block of iron for different radial distances from the primary proton beam line.

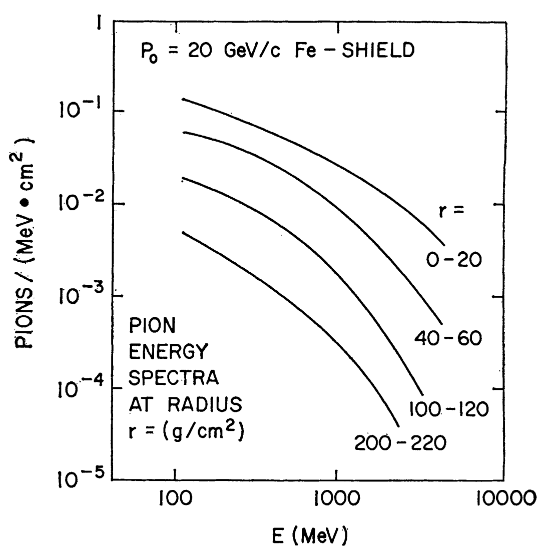

FIG. 17. Calculated pion energy spectra in a block of iron for different radial distances from the primary proton beam line.

iron block. The cascade was excited by a 20 GeV/c proton beam. The neutrons are the most important components in the cascade. It is difficult to compare these curves with corresponding experimental particle spectra. Cosmic-ray neutron spectra are expected to be different in the region of the high energies considered. The primary spectrum is

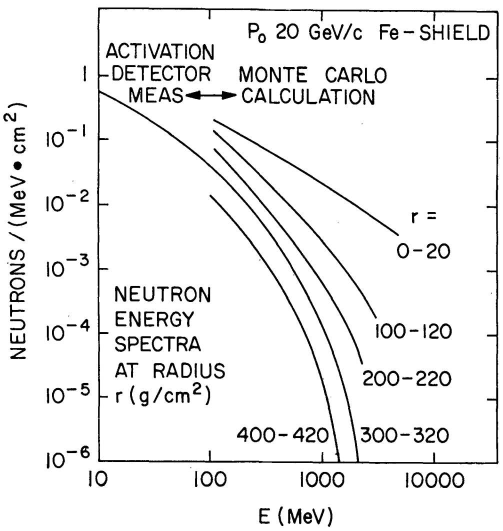

FIG. 18. Calculated neutron energy spectra in a block of iron for different radial distances from the primary proton beam line. The curve for $r = 300$ to 320 g/cm^2 is continued down to $E = 10$ MeV by using the ring-top neutron spectrum of Ref. 4.

different and extends to much higher energies than 20 GeV, and the same must be true for the neutron spectra at sea level. Neutron energy spectra around accelerators, evaluated from activation detector measurements as in Ref. 7, cannot be expected to be significant much above $E = 100$ MeV even if the curves are continued up to much higher energies, as was done in Ref. 4. There seems to be no physical process that could be responsible for the transmission, through thick lateral shields, of neutrons with energies nearly equal to the primary proton energy, but many such neutrons are present according to the spectra in Ref. 4.

Below 100 MeV, however, the experimental neutron spectra are expected to be much better, and those of Ref. 7 are used to continue the calculated energy spectra from $E = 100$ MeV (about the lowest energy for which the spectra can at present be calculated by Monte Carlo methods) down to lower energies. This was done with typical activation detector spectra for one of the curves in Fig. 18.

4.4. *The Energy Deposition of the Hadronic Cascade*

4.4.1. *Comparison with Total Absorption Detector Measurements.* Table 4.III gives the percentages of the total energy deposited for 8 and 100 GeV protons resulting from ionization energy losses of charged particles, electromagnetic cascades from π^0 mesons, excitation energy according to the definition given in Sec. 2, and particles created with $E < E_{\text{thr}}$.

TABLE 4.III
Percentages of the incident proton energy deposited in the cascade by the various mechanisms

p_0 [GeV/c]	8	20	50	100	300
Ionization	24	22	19.5	17	15.5
π^0 Mesons	27	36	43.5	50.5	56
Excitation	45	39	34.5	30	26.5
Particles with $E < E_{\text{thr}}$	4	3	2.5	2.5	2

Table 4.III confirms the assumption that the particles with $E < E_{\text{thr}}$ are relatively unimportant. At a few GeV the excitation energy contribution is the most important, but at higher energy the electromagnetic cascades take over.

The comparison of the histogram of the energies deposited by each single incoming proton in a block of a certain size with total absorption detectors is a good method to check the energy deposition mechanisms used in the calculation against experiments. In Fig. 19 we compare with TANC-detector measurements of Hughes *et al.*[126] Since the calculation is for incoming protons and the experiment used pions, no complete agreement can be expected. In the Monte Carlo calculation, on the average, 53 per cent of the energy was deposited against 49 per cent according to the measurements. The width of the peaks is comparable, and only the position of the maximum differs somewhat.

The calculated curve given in Fig. 19 compares similarly well with SANC-detector measurements.[127]

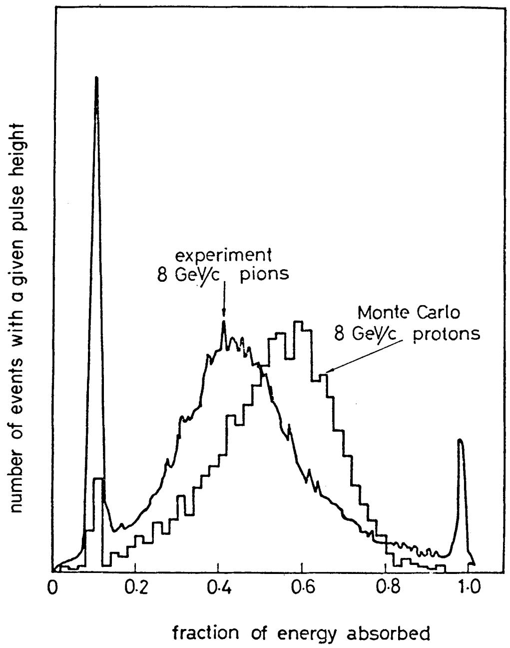

FIG. 19. The pulse height distribution of 8 GeV/c pions in a NaI(TL) TANC detector of $r = 14$ cm and $1 = 140$ cm measured by Hughes *et al.* The measured curve is compared with the results of the Monte Carlo calculation for 8 GeV/c protons. The sharp peak near the origin is due to protons (in the calculation) and pions and muons (in the experiment) traversing the detector without nuclear interaction. The sharp peak near to 1 is due to electrons.

4.4.2. *Comparisons with Target Heating and Radiation Doses on Magnet Units in Proton Synchrotrons.* The energy deposition of the hadronic cascade also leads to a heating of the material. This is especially important for devices which interact with the full primary proton beam, such as targets, beam dumps, and collimators. We calculate the temperature rise ΔT(°C) of the materials using the densities ρ, heat capacities C_p, and the relations:

$$1 \text{ GeV} = 1.6 \cdot 10^{-3} \text{ erg} = 1.6 \cdot 10^{-10} \text{ J}$$
$$= 0.383 \cdot 10^{-10} \text{ cal}. \tag{4.4}$$

If E is the calculated energy deposition in GeV/(cm^3, incoming proton) we get the heat Q in cal/(g, proton)

$$Q = 0.383 \cdot 10^{-10} \frac{E}{\rho} \tag{4.5}$$

and the instantaneous temperature rise ΔT by the interaction of a short beam pulse, measured in °C/(10^{12} protons)

$$\Delta T = 38.3 \frac{E}{\rho \cdot C_p}. \tag{4.6}$$

The energy deposition is calculated by FLUTRA as function of the co-ordinates Z (along the beam axis) and r (perpendicular to the beam axis). Henny and Potier *et al.*[128,129] measured the heat deposited by proton beams (10^{12} protons) of 12 and 24 GeV/c and about 6 mm diam. in a Cu target of 12 mm diam. and 80 mm length. These results compare well with the results of the FLUTRA calculation.

P_0	experimentally[128,129]	FLUTRA[44]
12 GeV/c	24 cal	29.4 cal/10^{12} p
21 GeV/c	—	42.3 cal/10^{12} p
24 GeV/c	37.5 cal	44.5 cal/10^{12} p

We wish to emphasize that only about 6 cal/(10^{12} protons) results from the ionization by the primary protons in the beam, and most of the heat deposited comes therefore from the cascade.† Using the same programme one calculates for a 300 GeV proton beam of 10^{13} particles hitting a 2×2 mm^2 Cu target an instantaneous temperature rise of about 1000 °C.

The energy deposition density calculated with the programme MAGTRA was compared with radiation doses measured on the front faces of synchrotron magnets downstream of internal targets in Refs. 38, 41 and 45. The energy density is related to radiation dose using the relations:

$$1 \text{ rad} = 10^2 \text{ erg/g}$$
$$1 \text{ GeV/g} = 1.6 \cdot 10^{-5} \text{ rad}. \tag{4.7}$$

The results of the calculation agree with experimental results[130-133] within a factor 2–3 as can be judged from Fig. 20.

† There is no contradiction to the values given in Table 4.III, which refer to the energy deposition in a large end stop where the cascade is fully developed. The 6 cal/44.5 cal should not give 22 per cent. The percentages of energy deposited by the different mechanisms in a small target where the cascade is only weakly developed differ from the values in Table 4.III.

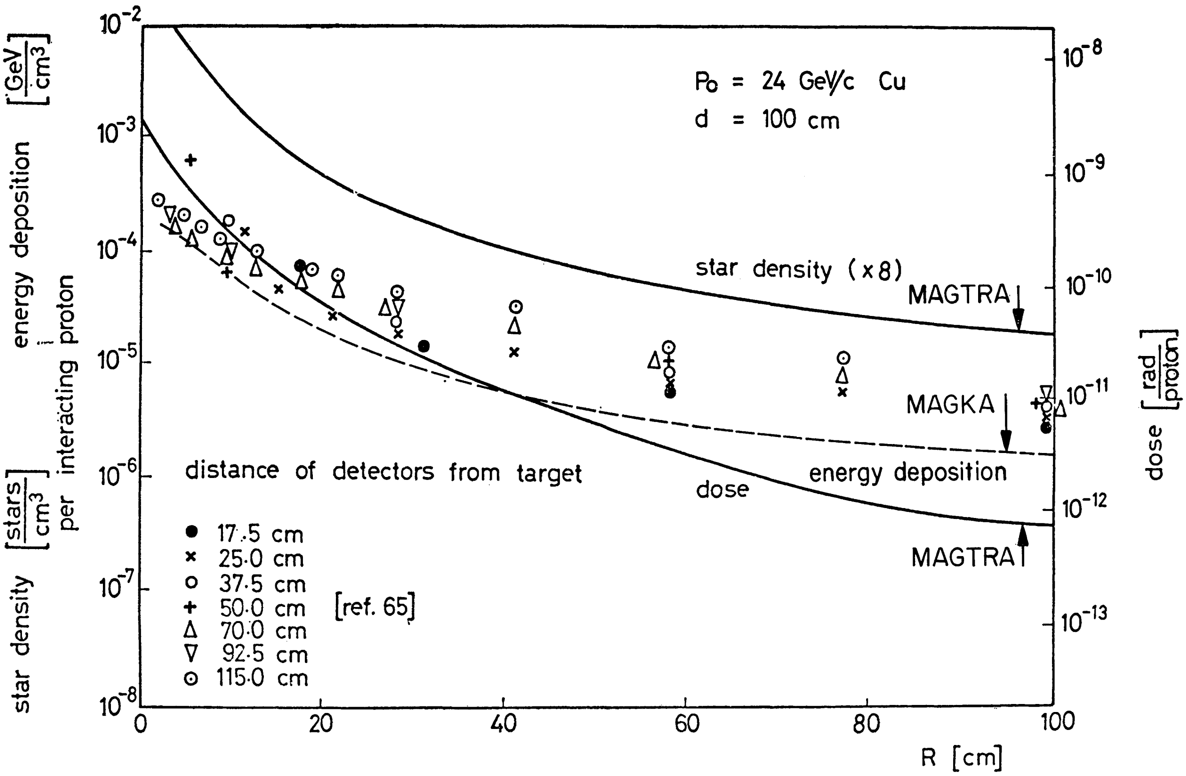

FIG. 20. Comparison of calculated and measured[133] doses at $p_0 = 24$ GeV/c on a plane perpendicular to the proton beam at 100 cm downstream the target. Also given is the star density multiplied by a factor 8. The energy deposition curve calculated with the new computer programme MAGKA using the new formulae for secondary particle production (2.15) and (2.14) agrees much better in shape with the measured angular distribution than the curve obtained with the old programme MAGTRA which uses the formulae (2.12) and (2.13).

4.5. *Comparison with the Hadronic Cascade Star Densities with Induced Activities*

The computer programmes mentioned TRANSK, FLUTRA, MAGTRA, etc. ... calculate besides other things the hadronic cascade star densities (HCSD) which refer to stars produced by hadrons of energy greater than about 100 MeV.

Hadrons, mainly neutrons also with energy lower than this cut-off in the calculation, contribute to the production of induced activity. Comparing with activation detector measurements, using the neutron energy spectra determined from these measurements as well as the ones determined in the Monte Carlo calculation, we found[7,36] that between 3 to 6 times more particles contribute to the measured C and Al activation, than were considered in the calculation. It is therefore not very useful to calculate the isotope production in the stars from the Monte Carlo calculation, as this would not give the isotopes produced by lower energy particles. However, at most positions the hadronic cascade is in equilibrium, which means that the particle energy spectra are nearly independent of the position. Therefore the distribution of radioactive nuclei produced by spallation is expected to have nearly the same shape as the calculated star density. We therefore assume that generally the calculated HCSD are proportional to the distribution of the radioactive nuclei, and furthermore to the γ dose rate resulting from the decay of these nuclei.

To be specific, the quantity found in the Monte Carlo calculation which will be considered here is S, the HCSD in Fe measured in stars/(cm^3 sec primary interaction). The quantity we are interested in is D, the distribution of dose rate measured in contact with a semi-infinite solid material, in units of rem/h, for a given irradiation time t_i and a given cooling time t_c after the end of irradiation. We use mostly $t_i = 30$ days and $t_c = 1$ day. It is easy to predict the dose rates for different

t_i and t_c. Both quantities are assumed to be proportional

$$D = \omega \cdot S \tag{4.8}$$

and we have to determine the parameter ω empirically. ω was determined in Ref. 42 by comparison with calculations by Armstrong and Alsmiller[48] and by Barbier[134] as well as by comparison with experimental and operational experience around the CPS.

Armstrong and Alsmiller[48] calculate the time dependent photon dose rates from induced radioactivity with the Monte Carlo method. They assume an infinite cylinder of iron and protons interacting uniformly along the centre line of the cylinder (an approximation of proton losses on the vacuum chamber of accelerator magnets).

We compare their dose rate distributions for $t_i = \infty$ and $t_c = 0$ in Fig. 1 with the HCSD calculated under identical assumptions with the programme MAGTRA. The shapes of the curves agree well and we obtain by comparison

$$\omega_{\infty,0} = 5 \cdot 10^{-6} \frac{\text{rem/h}}{\text{stars/(cm}^3\text{ sec)}} \tag{4.9}$$

from which it follows using Fig. 6 or Ref. 48 for $t_i = 30$ days and $t_c = 1$ day,

$$\omega_{30,1} = 1.2 \cdot 10^{-6} \frac{\text{rem/h}}{\text{stars/(cm}^3\text{ sec)}}. \tag{4.10}$$

Other comparisons lead to lower conversion factors.[42]

Sullivan found the value[135]

$$\omega_{30,1} = 0.5 \cdot 10^{-6} \frac{\text{rem/h}}{\text{stars/(cm}^3\text{ sec)}}. \tag{4.11}$$

But we feel it is safe to use (4.10) for predictions of dose rates for our HCSD calculations. The resulting dose rate should be conservative.

4.6. *Muon Fluxes Resulting from the Hadronic Cascade*

The problem of muon shielding was treated by several authors.[147-151] In these calculations one assumes usually a target, where pions and kaons are created, followed by a decay path, where the pions and kaons decay into muons, and finally a muon shield, where only the attenuation of the muons is studied. Such calculations were also used to study the muon shielding problem in the case of a proton beam end stop[147] by representing the muons, which result in reality from the decay of pions and kaons inside the end stop by muons resulting from an 'effective decay path' of $1.8\lambda_{abs}$. We do not consider here the muon shielding problem in the presence of a decay path where no hadronic cascade calculation is necessary.

We consider here only a proton beam hitting an end stop. Muons are created in this case by the decay of cascade pions and kaons within the shielding material. No effective decay path approximation is necessary in the cascade calculation.

The total flux density (this is the sum of proton, neutron, pion and muon fluxes) in steel for depths less than 2000 to 2500 g/cm² or about 3 m Fe is essentially determined by the fluxes of the strongly interacting particles (protons, neutrons and pions) alone. For depths larger than this the muon flux

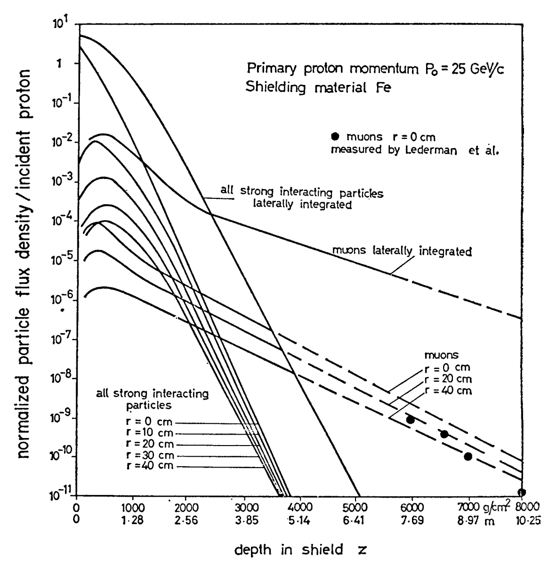

FIG. 21. Longitudinal development of strongly interacting particle and muon flux densities of a nucleon meson cascade initiated by a well collimated proton beam of momenta $p_0 = 25$ GeV/c in Fe. All curves are normalized to unit proton flux density at $r = 0$ and $z = 0$. Calculated curves are given for the laterally integrated fluxes and for the flux densities on ($r = 0$) and outside ($r \neq 0$) the beam axis. The calculated muon flux densities along the beam axis are compared with experimental values obtained by Burns *et al.*[67,68] These measurements were done at $p_0 = 20$ and 30 GeV/c. The values for $p_0 = 25$ GeV/c have been obtained by interpolation. The first metre of shield used consisted of Pb followed by about 10 m Fe. To compare with the calculated values in the pure Fe shield, we replaced the 1 m Pb by the corresponding number of interaction length of Fe.

dominates. This can be seen from Fig. 21 which gives the calculated and extrapolated longitudinal density curves for the strongly interacting particles and for the muons in Fe. The laterally integrated densities and the densities on and outside the beam axis are given. The muon fluxes along the beam axis in Fe at depths between 6000 and 8000 g/cm^2 can be compared with experimental results obtained by Burns *et al.*[136,137] The experimental values for the muon densities along the beam axis are shown in Fig. 21 and agree rather well with the calculated densities.

5. ANALYTIC CALCULATION OF THE HADRONIC CASCADE

Analytical solutions of the one-dimensional transport equation of the nucleus–meson cascade in slab geometry were given by Passow,[10] Alsmiller *et al.*,[11–17] Barbier[28] and O'Brien.[19–24] O'Brien[23] used the transport equation in the form:

$$\left[\mu\frac{\partial}{\partial r}+\sigma_j(E)+\delta_{nj}\,\sigma_{Ej}(E)+\frac{\delta_{\pi^\pm j}+\delta_{K^\pm j}}{(P_j/m_j)c\tau_j\,p}-(1-\delta_{nj})\frac{\partial}{\partial E}S_j(E)\right]\varphi_{sj}(r,E,\mu)$$
$$=\sum_{k=p,n,\pi^\pm K^\pm}\int_{-1}^{1}\mathrm{d}\mu'\int_{E}^{E_{\max}}\mathrm{d}E_B\,F^t_{jk}(E_B,E,\mu'\to\mu)$$
$$\cdot\left[\varphi_{sj}(r,E_B,\mu')+\varphi_{ij}(r,E_B,\mu')\right],\qquad (j,k=p,n,\pi^\pm,K^\pm)\qquad(5.1)$$

where

p, n, $\pi^\pm$, $K^\pm$ = protons, neutrons, charged pions and charged kaons, respectively,

r = depth, in units of g/cm^2, in the slab,

μ = cosine of the angle with respect to the normal of the slab,

$\varphi_{sj}(r, E, \mu)$ = flux per MeV of secondary particles of type j ($j = p, n, \pi^\pm K^\pm$),

$\varphi_{ij}(r, E, \mu)$ = flux of primary particles of type j,

P_j = momentum of particle of type j in units of GeV/c,

m_j = rest mass of particle of type j in units of GeV/c^2,

E = energy of flux in GeV,

τ_j = mean life (in CM) of particle of type j,

c = velocity of light (in vacuo),

$\sigma_j(E)$ = non-elastic cross section for particles of type j, in cm^2/g,

$\sigma_{Ej}(E)$ = elastic scattering cross section for neutrons, in units of cm^2/g,

$S_j(E)$ = stopping power of particles of type j in MeV cm^2/g,

$F^t_{jk}(E_B, E, \mu' \to \mu)$ = number of particles of type j per unit energy about E per unit solid angle traveling in a direction μ arising from a nuclear collision with a particle of type k ($k = p$, n, $\pi^\pm$, $K^\pm$) traveling in the direction μ' and having energy E_B.

$F^t_{jk}(E_B, E, \mu' \to \mu)$ = has 2 components, and may be written

$$F^t_{jk}(E_B,E,\mu'\to\mu)=F^{\mathrm{nel}}_{jk}(E_B,E,\mu'\to\mu)\sigma_j(E_B)+F^{\mathrm{el}}_{jk}(E_B,E,\mu'\to\mu)\sigma_{Ej}(E_B)$$

where F^{nel}_{jk} and F^{el}_{jk} correspond to nonelastic and elastic processes.

Severe approximations and simplifications are necessary to find solutions for the fluxes, some of which are

(i) neglecting elastic scattering and ionization energy losses,
(ii) assuming constant absorption cross sections,
(iii) assuming all secondary particle production to be in forward direction and to be represented by a rather simple formula.

The results of the calculations[13,15,23] agree well with experimental data and with Monte Carlo conclusions. Figure 22[23] gives the laterally integrated star density at $p_0 = 19.2$ GeV calculated by O'Brien and compared with experimental results[1] and with the Monte Carlo calculation. There is good mutual agreement.

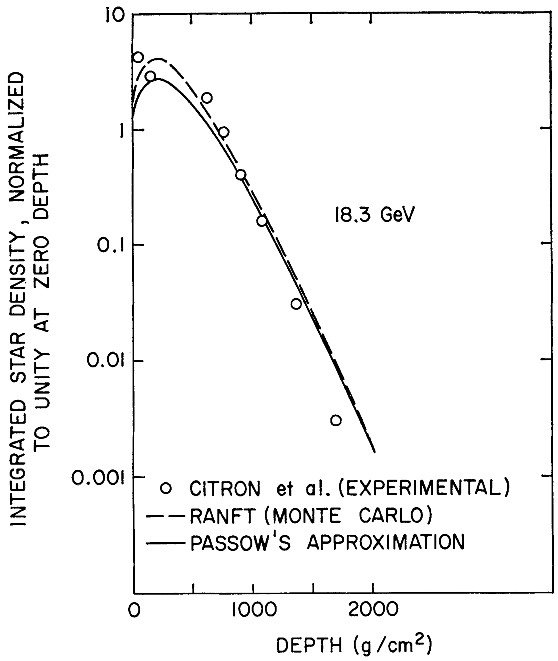

FIG. 22. The laterally integrated star density in nuclear emulsion with depth produced by an 18.3 GeV proton beam normally incident on an iron slab. The measurements were made by Citron *et al.*[1]

O'Brien and McLaughlin[19–22,24,25,27] describe an analytic cascade calculation of the neutron spectrum below 500 MeV. They represent the neutron flux at depth r with energy E and direction cosine μ as a sum of four Legendre polynominals:

$$\varphi_N(r, E, \mu) \sim \sum_{L=0}^{3} \tfrac{1}{2}(2L+1)F_L(r, E)P_L(\mu) \qquad (5.2)$$

where

r = depth in shield (g/cm^2);
μ = the cosine with respect to the normal direction of the shield;
$\varphi_N(r, E, \mu)$ = the flux of neutrons per MeV at a depth r, having an energy E, and a direction cosine μ;
$P_L(\mu)$ = the Legendre polynomials of order L;
$F_L(r, E)$ = the Legendre coefficients of the flux.

These essentially one-dimensional calculations can be extended to cylindrical or spherical geometry and therefore used for shielding calculations for linear and circular accelerators. The upper energy limit and the neglect of the meson and proton components restrict the applicability to the transverse shielding. Due to the finite transverse momenta of all produced secondaries, the energy range treated is sufficient to calculate the transverse development of the cascade for even the highest energy accelerators.

The results of these calculations were extensively compared with experimental values and Monte Carlo calculations and it has been established that the results are in very good agreement. As an example, Fig. 23 compares the results of the calculations[24] with experimental results.[5]

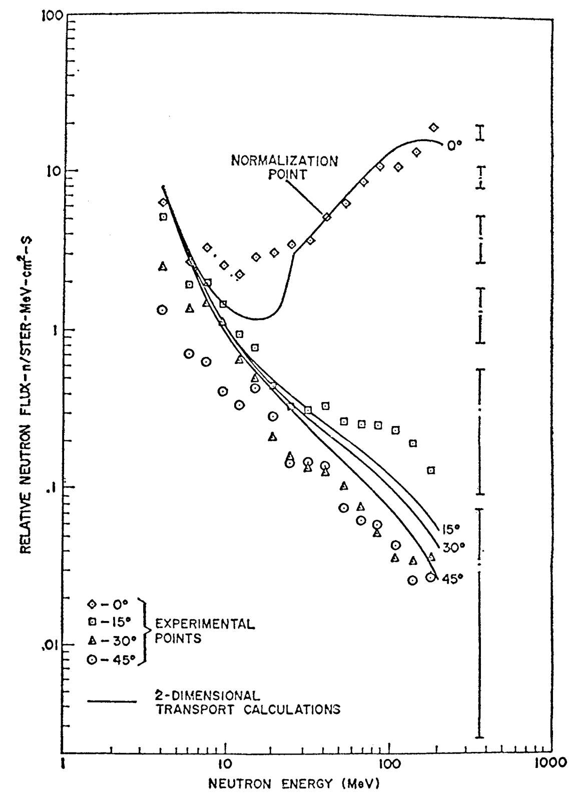

FIG. 23. Experimental and theoretical determination of the distribution of neutrons in energy and angle per steradian emerging from a 40 cm iron slab irradiated by a gun source made from the 49° neutron beam of the Princeton–Pennsylvania Accelerator. The error bars at the right of the graph are roughly the same size for a given ordinate. Calculations are for performed the centre of the neutron distribution, $r = 0$.

ACKNOWLEDGEMENTS

The Monte Carlo methods and applications reported would never have been developed without the discussions and suggestions of Dr. J. A. Geibel, Dr. L. C. W. Hobbis, Dr. K. Goebel, Dr. M. Awschalom, Dr. L. Hoffmann, Dr. R. H. Thomas, Dr. G. R. Stevenson as well as other members of 300 GeV study groups.

REFERENCES

1. A. Citron, L. Hoffmann, C. Passow, W. R. Nelson and M. Whitehead, *Nucl. Instr. Meth.*, **32,** 48 (1965).
2. R. L. Childers, C. D. Zerby and C. M. Fisher, *Nucl. Instr. Meth.*, **32,** 53 (1965).
3. A. R. Smith, 'Some Experimental Shielding Studies at the 6.2 BeV Berkeley Bevatron,' Lawrence Radiation Laboratory Report UCRL-16323 (1965).
4. W. S. Gilbert, D. Keefe, J. B. McCaslin, H. W. Patterson, A. R. Smith, L. D. Stephens, K. B. Shaw, G. R. Stephenson, R. H. Thomas, R. D. Fortune and K. Goebel, '1966 CERN-LRL-RHEL Shielding Experiment at the CERN Proton Synchrotron,' Lawrence Radiation Laboratory Report UCRL-17941 (1968).
5. F. Haynal, M. Awschalom, B. G. Bennett, J. E. McLaughlin, K. O'Brien, P. D. Raft and W. Schimmerling, 'A Study of the Neutron Cascade in Iron,' Princeton-Pennsylvania Accelerator Report PPAD 650 E (1968).
6. V. E. Aleinikov, V. N. Lebedev, V. Mautseva, M. I. Salatskaya, 'Attenuation by Concrete of the Neutron Flux Emitted at 90° to the Direction of the Primary Proton Beam of the 10 GeV Synchrophasotron,' JINR Dubna Report P-9-2933.
7. K. Goebel and J. Ranft, 'Radiation Measurements Around a Beam Stopper Irradiated by 19.2 GeV/c Protons, and Neutron Energy Spectra by Monte Carlo Nucleon-Meson Cascade Calculations,' Report CERN-70-16 (1970).
8. H.W. Patterson and R. H. Thomas, *Particle Accelerators*, **2,** 77 (1971).
9. K. Goebel (editor), 'Radiation Problems Encountered in the Design of Multi-GeV Research Facilities,' CERN Report CERN 71-21 (1971).
10. C. Passow, 'Phänomenologische Theorie zur Berechnung einer Kaskade aus schweren Teilchen (Nukleonenkaskade) in der Materie,' DESY Notiz A 2.85 (unpublished), Hamburg (1962).
11. R. G. Alsmiller, Jr., F. S. Alsmiller and J. E. Murphy, 'Nucleon-Meson-Cascade Calculation; Transverse Shielding for a 45 GeV Electron Accelerator (Part I),' Oak Ridge National Laboratory Report ORNL-3289 (1962).
12. R. G. Alsmiller, Jr. and F. S. Alsmiller, 'A Perturbation Method for Solving the Angle Dependent Nucleon-Meson Cascade Equations,' Report ORNL-3467 (1963).
13. R. G. Alsmiller, Jr. and J. E. Murphy, 'Nucleon-Meson Cascade Calculations: The Star Density Produced by a 24 GeV Proton Beam in Heavy Concrete,' Report ORNL-3367 (1963).
14. R. G. Alsmiller, Jr., 'A Solution to the Nucleon-Meson Cascade Equations Under Very Special Conditions,' Report ORNL-3570 (1964).
15. R. G. Alsmiller, Jr. and J. Barish, 'Calculation of the Nuclear Cascade in Steel Initiated by 10 and 19.2 GeV/c Protons and Comparison with Experiment,' Report ORNL-TM-1072 (1965).
16. F. S. Alsmiller, 'A General Category of Soluble Nucleon-Meson Cascade Equations,' Report ORNL-3746 (1965).
17. R. G. Alsmiller, Jr., 'Shielding Calculations for High Energy Accelerators.' Paper presented at the I Symposium on Accelerator Radiation Dosimetry and Experience, Brookhaven National Laboratory, 1965; Report ORNL-TM-1298 (1965).
18. R. J. Riddell, Jr., 'High Energy Nuclear Cascades in Matter,' Lawrence Radiation Laboratory Report UCRL-11989 (1965).
19. K. O'Brien, 'Tables for the Determination of the Lateral Shielding Requirements of High Energy Accelerators,' USAEC Health and Safety Laboratory Report HASL-203 (1968).
20. K. O'Brien and J. E. McLaughlin, *Nucl. Instr. Meth.*, **60,** 129 (1968).
21. K. O'Brien, 'Transverse Shielding Calculations for the Components of a 0.5 TeV Proton Synchrotron,' USAEC Health and Safety Laboratory Report HASL-199 (1968).
22. K. O'Brien, *Nucl. Instr. Meth.*, **70,** 349 (1969).
23. K. O'Brien, *Nucl. Instr. Meth.*, **72,** 93 (1969).
24. K. O'Brien, *Proc. II Int. Conf. on Accelerator Dosimetry and Experience, Stanford*, **1969**, p. 253.
25. R. G. Alsmiller, Jr., *ibid.*, p. 166.
26. K. O'Brien, 'Shielding Calculations for Broad Neutron Beams Normally Incident on Slabs of Concrete,' USAEC Health and Safety Laboratory Report HASL-221 (1970).
27. K. O'Brien, *Nucl. Instr. Meth.*, **86,** 217 (1970).
28. M. Barbier and R. Hunter, 'Systematics of Extra-Nuclear Hadron Cascades in Shields,' Report CERN 71-13 (1971).
29. J. A. Geibel and J. Ranft, *Nucl. Instr. Meth.*, **32,** 65 (1965).
30. J. Ranft, 'Monte Carlo Calculation of the Nucleon-Meson Cascade in Shielding Materials Initiated by Incoming Proton Beams with Energies Between 10 and 1000 GeV,' Report CERN 64-47 (1964).
31. J. Ranft, *Nucl. Instr. Meth.*, **48,** 133 (1967).
32. J. Ranft, *Nucl. Instr. Meth.*, **48,** 261 (1967).
33. J. Ranft, 'Monte Carlo Calculation of the Nucleon-Meson Cascade. Calculation of Strongly Interacting Particle and Muon Fluxes at Very Large Depths Inside the Shielding Material and Comparison With Experimental Data,' CERN Internal Report MSP/Int.MU/EP 66-6 (1966).
34. J. Ranft, 'Improved Monte Carlo Calculation of the Nucleon-Meson Cascade in Shielding Materials,' CERN Internal Report MPS/Int.MU/EP 66-8 (1966).
35. J. Ranft, 'Monte Carlo Calculation of the Nucleon-Meson Cascade in a Block of Shielding Material. Attenuation of Strong Interacting Particle Densities Perpendicular to the Direction of the Primary Beam,' CERN Internal Report MPS/Int.MU/EP 67-1 (1967).
36. J. Ranft, 'Monte Carlo Calculation of Particle Loss

Distributions Along the Vacuum Chamber of the CPS Near Internal Targets and of the Transverse Attenuation of Strongly Interacting Particle Fluxes in the PS. Magnet Units and Earth Shield,' CERN Internal Report MPS/Int.MU/EP 67-5 (1967).
37. J. Ranft, 'Monte Carlo Nucleon-Meson Cascade Calculation in a Block of Shielding Material. Description of the Computer Programme TRANSK,' CERN Internal Report MPS/Int.MU/EP 67-6 (1967).
38. J. Ranft, 'Radiation Doses on Synchrotron Magnets by Monte Carlo Nucleon-Meson Cascade Calculations,' Rutherford High Energy Laboratory Internal Report Nimrod (BP) 69-57 (1969).
39. J. Ranft and T. Borak, 'Improved Nucleon-Meson Cascade Calculations,' National Accelerator Laboratory Internal Report PN-193 (1969).
40. J. Ranft, *Nucl. Instr. Meth.*, **81,** 29 (1970).
41. J. Ranft, 'Monte Carlo Calculation of Radiation Doses on Synchrotron Magnets, Further Comparison with Experimental Data,' Sektion Physik, Karl-Marx-Universität, Leipzig, Preprint TUL 29 (1970), unpublished.
42. J. Ranft and K. Goebel, 'Estimation of Induced Radioactivity Around High Energy Accelerators from Hadronic Cascade Star Densities (HCSD) Obtained from Monte Carlo Calculations,' Report CERN-HP 70-92 (1970).
43. K. Goebel and J. Ranft, 'Transverse Shielding for the 300 GeV Proton Synchrotron and the Transfer Tunnel up the West Area Target Station,' Report CERN-HP 70-91 (1970).
44. J. Ranft, 'Monte Carlo Cascade Calculation of Target Heating by the Proton Beam,' Sektion Physik, Karl-Marx-Universität, Leipzig, TUL 38 (1970).
45. J. Ranft, 'Radiation Doses on Synchrotron Magnets and Around Target Stations,' TUL 39 (1970).
46. D. C. Irving, R. M. Freestone and F. B. K. Kam, 'OSR, A General Purpose Monte Carlo Neutron Transport Code,' Oak Ridge National Laboratory Report ORNL-3622 (1965).
47. T. W. Armstrong and J. Barish, 'Calculation of the Residual Photon Dose Rate due to the Activation of Concrete by Neutrons from a 3 GeV Proton Beam in Iron,' Report ORNL-TM-2630 (1969).
48. T. W. Armstrong and R. G. Alsmiller, Jr., 'Calculation of the Residual Photon Dose Rate Around High Energy Accelerators,' Report ORNL-TM-2498 (1969).
49. H. Göllnitz, E. Heidebreder, K. Pinkau, C. Reppin and V. Schönfelder, *Nucl. Instr. Meth.*, **74,** 109 (1969).
50. V. N. Akimov, I. N. Fetisov, A. E. Morozov and S. A. Slavatinsky, 'The Investigation of the Nuclear Cascade Process in an Ionization Calorimeter,' Lebedev Physical Institute Preprint No. 141 (1969).
51. W. E. Kinney, 'The Nucleon Transport Code NTC,' Report ORNL-3610 (1964).
52. D. C. Irving, H. S. Moran and W. E. Kinney, 'Modification and Further Development of the Nucleon Transport Code NTC,' Report ORNL-TM-1866 (1969).
53. W. A. Coleman and T. W. Armstrong, 'The Nucleon-Meson Transport Code NMTC,' Report ORNL-4606 (1970).
54. T. A. Gabriel, 'Calculation of the Long Lived Induced Activity in the Soil Around High Energy Accelerator Target Areas,' Report ORNL-TM-3033 (1970).
55. R. G. Alsmiller, Jr., T. W. Armstrong and B. L. Bishop, 'The Absorbed Dose and Dose Equivalent from Negatively and Positively Charged Pions in the Energy Range 10 to 2000 MeV,' Report ORNL-TM-3105 (1970).
56. W. V. Jones, *Phys. Rev.*, **187,** 1868 (1969).
57. W. V. Jones, *Phys. Rev.*, **D1,** 2201 (1970).
58. T. A. Gabriel, R. G. Alsmiller, Jr. and J. Barish, 'Calculation of the Long Lived Induced Activity in the Soil Around High Energy Accelerator Target Areas, II,' Report ORNL-4599 (1970).
59. A. van Ginneken, 'Hadron Shielding Calculations: Effects of Voids,' National Accelerator Laboratory Report TM-287 (1971).
60. V. S. Barashenkov, N. M. Sobolevsky and V. D. Toneev, 'Interaction of High-Energy Radiation with Substance,' Dubna Preprint P2-5719 (1971).
61. J. V. Allaby, Yu. B. Bushnin, S. P. Denisov, A. N. Diddens, R. W. Dobison, S. V. Donskov, G. Giacomelli, Yu. P. Gorin, A. Klovning, A. I. Petrukhin, Yu. D. Prokoshkin, R. S. Shuvalov, C. A. Stahlbrandt and D. A. Stoyanova, 'Measurements of Total Cross Sections for Negative Particles on Protons in the Momentum Range 20–65 GeV/c,' submitted to the Lund Conference (1969).
62. G. D. de Meester, 'Measurements of Proton-Proton and Proton-Iron Inelastic Cross Sections Using Charged Cosmic Ray Hadrons of Energy Greater than 70 GeV,' Michigan University Report UM-HE-71-5 (1971).
63. N. L. Grigorov, V. E. Nesterov, F. D. Rapoport, I. A. Savenko and G. A. Skuridin, *Jadernaja Fisika*, **11,** 814 (1970).
64. G. B. Jodh, J. R. Wayland and Y. Pal, 'Behaviour of Inelastic Nucleon-Nucleus Cross Sections from 10^2 to 10^5 GeV,' University of Maryland preprint (1970).
65. V. S. Barashenkov, K. K. Gudima and V. D. Toneev, 'Energy Dependence of the Nuclear Cross Sections for Nucleons at Energy Above 50 MeV,' Dubna Report P2-4183 (1968).
66. V. S. Barashenkov, K. K. Gudima, A. S. Iljinov and V. D. Toneev, 'Energy Dependence of the Interaction Cross Section of π-Mesons with the Atomic Nuclei at Energies More than 50 MeV,' Dubna Report P2-4520 (1969).
67. G. Giacomelli, P. Pini and S. Stagni, 'A Compilation of Pion Nucleon Scattering Data,' Report CERN-HERA 69-1 (1969).
68. G. Giacomelli, 'A Compilation of Total and Total Elastic Cross Sections,' Report CERN-HERA 69-3 (1969).
69. J. D. Hansen, D. R. O. Morrison, N. Tovey and E. Flaminio, 'Compilation of Cross Sections, I—Proton Induced Reactions,' Report CERN-HERA 70-2 (1970).
70. E. Flaminio, J. D. Hansen, D. R. O. Morrison and N. Tovey, 'Compilation of Cross Sections, IV—π^+ Induced Reactions,' Report CERN-HERA 70-5 (1970).
71. E. Flaminio, J. D. Hansen, D. R. O. Morrison and N. Tovey, 'Compilation of Cross Sections, VI—π^- Induced Reactions,' Report CERN-HERA 70-7 (1970).

72. O. Benary, L. R. Price and G. Alexander, 'NN and ND Interactions (Above 0.5 GeV/c)—a Compilation,' Lawrence Radiation Laboratory Report UCRL 20000 NN (1970).
73. G. Bellettini, G. Cocconi, A. N. Diddens, E. Lillethun, G. Matthiae, J. P. Scanlon and A. M. Wetherell, *Nucl. Phys.*, **79**, 609 (1966).
74. J. Engler, K. Horn, J. König, F. Mönnig, P. Schludecker, H. Schopper, P. Sievers and H. Ullrich, 'Total Neutron Cross-Sections on Hydrogen and Various Other Elements in the 4–15 GeV/c Range, 'submitted to 14th Int. Conf. on High-Energy Physics, Vienna, 1968 (CERN, Geneva, 1968).
75. L. W. Jones, M. J. Longo, J. R. O'Fallon and M. N. Kreisler, *Phys. Letters*, **27B**, 328 (1968).
76. J. Ranft, 'Scattering of Protons in Septa of Resonant Ejection Systems,' Rutherford High Energy Laboratory Report Nimrod (BP) 69-5 (1969).
77. R. Hagedorn and J. Ranft, *Suppl. Nuovo Cimento*, **6**, 169 (1968).
78. J. Ranft, *Phys. Letters*, **31B**, 529 (1970).
79. H. Grote, R. Hagedorn and J. Ranft, *Particle Spectra*, CERN, Geneva, 1970.
80. L. Caneschi and A. Pignotti, *Phys. Rev. Letters*, **22,** 1219 (1969).
81. C. Risk and J. H. Friedman, *Phys. Rev. Letters*, **27**, 353 (1971).
82. R. P. Feynman, *Phys. Rev. Letters*, **23,** 1415 (1969).
83. N. F. Bali, L. S. Brown, R. D. Peccei and A. Pignotti, *Phys. Rev. Letters*, **25**, 557 (1970).
84. J. Benecke, T. T. Chou, C. N. Yang and E. Yen, *Phys. Rev.*, **188,** 2159 (1969).
85. A. H. Mueller, *Phys. Rev.*, **D2**, 2963 (1970).
86. H. M. Chang, C. S. Hsue, C. Quigg and M. M. Wang, *Phys. Rev. Letters*, **26**, 672 (1971).
87. C. E. De Tar, K. Kang, C. I. Tan and J. H. Weis, *Phys. Rev.* **D4**, 425 (1971).
88. D. Gordon and G. Veneziano, *Phys. Rev.* **D3**, 2116 (1971).
89. G. Ranft and J. Ranft, *Fortschr. Physik* **19**, 393 (1971).
90. G. Cocconi, L. J. Koester and D. H. Perkins, Lawrence Radiation Laboratory Report UCRL-10022, p. 167 (1961).
91. G. Cocconi, *Nucl. Phys.*, **B28**, 343 (1971).
92. G. Trilling, Lawrence Radiation Laboratory Report UCID-10148 (1966).
93. J. Ranft, 'An Empirical Formula Representing the Production of Secondary Protons by Primary Protons Interacting with Nuclei,' CERN Internal Report MPS/Int.MU/EP 66-3 (1966).
94. J. Ranft, 'An Empirical Formula Which Fits the Spectra of Secondary π^+ and π^- Mesons Produced by Protons on Be Targets,' CERN Internal Report MPS/Int.MU/EP 66-4 (1966).
95. J. Ranft, 'The Computer Programme SPUKJ Calculating and Plotting Secondary Particle Fluxes According to the Thermodynamical Model and Empirical Formulae,' Sektion Physik, Karl-Marx-Universität, Leipzig, TUL 37 (1970).
96. J. V. Allaby, F. Binon, A. N. Diddens, P. Duteil, A. Klovning, R. Meunier, J. P. Peigneux, E. J. Sacharidis, K. Schlüpmann, M. Spighel, J. P. Stroot, A. M. Thorndike and A. M. Wetherell, Report CERN 70-12 (1970).
97. H. Bøggild, K. H. Hansen and M. Suk, *Nucl. Phys.*, **B27,** 1 (1971).
98. J. Ranft, 'An Empirical Formula, Describing Particle Production in Proton-Nucleus Collisions, which is Convenient for Monte Carlo Calculations,' Report CERN-Lab. II-Ra/Int. 71-7 (1971).
99. U. Fano, *Ann. Rev. Nucl. Sci.*, **13,** 1 (1963).
100. W. A. Barkas and M. J. Berger, NASA Publication SP-3013 (1964) (available through Clearinghouse for Federal Scientific and Technical Information, Springfield, Va. 22151, U.S.A.).
101. G. Bathow, E. Freytag and K. Tesch, *Nucl. Phys.*, **B2,** 669 (1967).
102. G. Bathow, E. Freytag, M. Koebberling, K. Tesch and R. Kajikawa, *Nucl. Phys.*, **B20**, 592 (1970).
103. J. Nishimura, 'Theory of Cascade Showers,' *Handbuch der Physik*, Vol. XLVI/2 Kosmische Strahlung II, ed. S. Flügge, Springer-Verlag, 1967.
104. J. Ranft, 'Calculation of Beam Loss Distributions and Radiation Doses on Magnets of Proton Synchrotrons,' *Proc. II Int. Conf. on Accelerator Dosimetry and Experience, Stanford, 1969*, p. 416.
105. J. Ranft, 'Scattering of 250 GeV/c Protons in a Wire Septum and in a Scraper,' Sektion Physik, Karl-Marx-Universität, Leipzig, TUL 27 (1970).
106. A. W. Maschke and K. R. Symon, 'Extraction System for the 200 GeV Accelerator,' *Proc. USSR National All-Union Conference on High Energy Accelerators, Moscow 1968*, p. 516.
107. C. Bovet, 'Variation des Parametres de l'Ejection Lente,' CERN Internal Report MPS/Int.DL/65-6 (1965).
108. J. Ranft, 'Absorption and Out-Scattering of High Energy Protons Hitting an Absorber at Small Angles,' Rutherford High Energy Laboratory Internal Report Nimrod (BP) 69-4 (1969).
109. J. Ranft, 'Monte Carlo Calculation of Particle Loss Distributions Along the Vacuum Chamber of the CPS Near Internal Targets,' CERN Internal Report MPS/Int.MU/EP 67-5 (1967).
110. J. Ranft, 'Beam Losses and Beam Scrapers in Proton Synchrotrons,' RHEL Internal Report Nimrod (BP) 69-9 (1969).
111. A. A. Garren and T. W. Eusebio, 'SYNCH, a Computer System for Synchrotron Design and Orbit Analysis,' Lawrence Radiation Laboratory Report UCID-10153 (1965).
112. E. J. N. Wilson, '450 GeV Within 1200 Metres Radius, a Separated Function Alternative to the 300 GeV Machine Lattice,' CERN Internal Report ISR-300/GS/68-22 (1968).
113. R. G. Alsmiller, Jr., T. W. Armstrong and W. A. Coleman, 'The Absorbed Dose and Dose Equivalent from Neutrons in the Energy Range 60 to 3000 MeV and Protons in the Energy Range 400 to 3000 MeV,' Oak Ridge National Laboratory Report ORNL-TM-2924 (1970).
114. T. A. Gabriel and R. T. Santoro, 'Calculation of the Long Lived Activity in Soil Produced by 500 GeV Protons,' ORNL-TM-3262 (1970).
115. R. T. Santoro and T. A. Gabriel, 'Nucleon and Pion Star Production from High Energy (>40 GeV) Protons Incident on Iron,' ORNL-TM-3335 (1971).
116. T. W. Armstrong, R. G. Alsmiller, Jr. and K. C. Chandler, 'Monte Carlo Calculations of High-Energy Nucleon-Meson Cascades and Application to Galactic Cosmic Ray Transport,' ORNL-TM-3319 (1971).

117. T. W. Armstrong and B. L. Bishop, 'Calculation of the Absorbed Dose and Dose Equivalent Induced by Medium Energy Neutrons and Protons and Comparison with Experiment,' ORNL-TM-3304 (1971).
118. T. W. Armstrong and J. Barish, 'Calculated Activities of Copper and Iron by 3 GeV Protons,' ORNL-TM-2902 (1970).
119. T. A. Gabriel, 'Calculation of the Long-Lived Induced Activity in Soil Produced by 200 MeV Protons,' ORNL-TM-2848 (1970).
120. T. W. Armstrong and J. Barish, 'Calculation of the Residual Photon Dose Rate Induced in Iron by 200 MeV Protons,' ORNL-TM-2583 (1969).
121. H. E. Bertini, 'Calculation of Nuclear Reactions for Incident Nucleons and π-Mesons in the Energy Range 30 to 2700 MeV,' *Proc. II Int. Conf. on Accelerator Dosimetry and Experience, Stanford, 1969*, p. 42.
122. V. S. Murzin, 'Principles and Applications of the Ionization Calorimeter,' *Progress in Elementary Particle and Cosmic Ray Physics*, Vol. IX, 247 (1967).
123. R. Hofstadter, *Nucl. Instr. Meth.*, **63,** 136 (1968).
124. R. Hofstadter, 'Total Absorption Detectors for High and Super High Energy Physics,' Stanford University Report HEPL 599 (1969).
125. E. B. Hughes, W. L. Lakin, I. Sick and R. Hofstadter, *Nucl. Instr. Meth.*, **75,** 130 (1969).
126. E. B. Hughes and R. Hofstadter, 'Total Absorption Detector,' Stanford University Report HEPL 631 (1970).
127. J. E. Pilcher and C. Rubbia, 'Sampling Total Absorption Detector (SANC) for Hadrons at High Energies,' Harvard University Preprint (1970).
128. L. Henny, A. Millich, J. P. Potier and G. Willemin, (Mesure de L'Apport de Chaleur par Faisceau,' CERN Internal Report MPS/CO/MD 70-14 (1970).
129. L. Henny, J. P. Potier and G. Willemin, 'Apport de Chaleur par Faisceau Dans une Cible Externe,' CERN Internal Report MPS/CO/MD 70-21 (1970).
130. R. Sheldon and G. Stapleton, unpublished results, personal communication (1969).
131. M. Van de Voorde, 'An Analysis of the Results of Megarad Dose and Flux Measurements at the CERN Internal Report ISR-MA/MV/vh (1969).
132. G. R. Stevenson, D. M. Squier and G. S. Levine, 'The Distribution of Dose and Induced Activity Around External Proton Beam Targets,' Rutherford High Energy Laboratory Report RHEL/MR-6 (1971).
133. G. S. Levine, D. M. Squier, G. B. Stapleton, G. R. Stevenson, K. Goebel and J. Ranft, 'The Distribution of Dose and Induced Activity Around External Proton Beam Targets,' RHEL Preprint RPP/R-9 (1971).
134. M. Barbier, *Induced Radioactivity*, North Holland, 1969.
135. A. H. Sullivan, 'An Approximate Relation for the Estimation of the Dose Rate from Radioactivity Induced in High Energy Particle Accelerators,' CERN Internal Report HP-71-96 (1971).
136. R. Burns, G. Danby, E. Hyman, L. M. Lederman, W. Lee, J. Rettberg and J. Sunderland, *Phys. Rev. Letters*, **15,** 830 (1965).
137. R. Burns, E. Hyman, L. Lederman, W. Lee, J. Rettberg, J. Sunderland and G. Danby, 'Search for Intermediate Bosons in Proton-Nucleon Collisions,' Columbia University Report NEVIS-153 (1966).
138. W. A. Coleman and R. G. Alsmiller, Jr., *Nucl. Sci. Eng.*, **34,** 104 (1968).
139. T. W. Armstrong and R. G. Alsmiller, Jr., *Nucl. Sci. Eng.*, **33,** 291 (1968).
140. G. Rudstam, *Z. Naturforsch.*, **21A,** 1027 (1966).
141. R. M. Sternheimer, *Phys. Rev.*, **88,** 851 (1952).
142. R. M. Sternheimer and R. F. Peierls, *Phys. Rev.*, **B3,** 3681 (1971).
143. J. Ranft and J. T. Routti, 'FLUKA and MAGKA, Monte Carlo programs for calculating nucleun-meson cascades in cylindrical geometries.' CERN LAB II–RA/71-4 (1971).
144. J. Ranft, 'Results of radiation dose calculations with the programs FLUKA and MAGKA and experimental results at 7 and 24 GeV/C.' CERN LAB II–RA/71-3 (1971).
145. R. H. Thomas, 'Energy Loss of High Energy Muons,' Lawrence Radiation Laboratory Report UCID-10010 (1964).
146. C. Richard-Serre, 'Evaluation de la Perte d'Energie Unitaire et du Parcours pour des Muons de 2 à 600 GeV Dans un Absorbant Quelconque,' Report CERN 71-18 (1971).
147. D. Keefe and C. M. Noble, *Nucl. Instr. Meth.*, **64,** 173 (1968).
148. E. Berthel, B. de Sereville, E. Freytag and H. Wachsmuth, 'Shielding Against Muons,' Report CERN 71-21, p. 79 (1971).
149. W. R. Nelson, *Nucl. Instr. Meth.*, **66,** 293 (1968).
150. R. G. Alsmiller, Jr., F. S. Alsmiller, J. Barish and Y. Sima, 'Muon Transport and the Shielding of High-Energy (500 GeV) Proton Accelerators,' Oak Ridge National Laboratory Report ORNL-TM-3353 (1971).
151. P. E. Kuhlmann and H. O. Wüster, 'Muon Shielding Calculations,' Report CERN-ECFA 66/WG 2/US-SG 5/PEK-HOW-1 (1966).

Received 24 September 1971
(and in revised form 17 November 1971)